LATVIAN JOURNAL of PHYSICS and TECHNICAL SCIENCES

ISSN 0868 - 8257

Institue of Physical Energetics-70

4

(Vol. 53)

2016

Ind. pasūt. € 1,50 Indekss 2091
Org. € 15,00 Indekss 2092

SATURS

ENERĢĒTIKAS FIZIKĀLĀS UN TEHNISKĀS PROBLĒMAS

ELEKTRONIKA

Price to individual subscribers € 1.50/issue Index 2091
Price to collective subscribers € 15.00/issue Index 2092

CONTENTS

PHYSICAL AND TECHNICAL ENERGY PROBLEMS

ELECTRONICS

Индивид. заказ. Є 1,50 Индекс 2091
Орг. заказ. Є 15,00 Индекс 2092

СОДЕРЖАНИЕ

ФИЗИКО-ТЕХНИЧЕСКИЕ ПРОБЛЕМЫ ЭНЕРГЕТИКИ

ЭЛЕКТРОНИКА

LATVIAN JOURNAL of PHYSICS and TECHNICAL SCIENCES

LATVIJAS FIZIKAS un TEHNISKO ZINĀTŅU ŽURNĀLS

ЛАТВИЙСКИЙ ФИЗИКО-ТЕХНИЧЕСКИЙ ЖУРНАЛ

Published six times a year since February 1964
Iznāk sešas reizes gadā kopš 1964. gada februāra
Выходит шесть раз в год с февраля 1964 года

4 (Vol. 53) • 2016

RĪGA

INDEKSĒTS (PUBLICĒTS) | INDEXED (PUBLISHED) IN

www.scopus.com
www.degruyter.com
EBSCO (Academic Search Complete, www.epnet.com), INSPEC (www.iee.org.com).
VINITI (www.viniti.ru), Begell House Inc/ (EDC, www.edata-center.com).

Izdevējs: Fizikālās enerģētikas institūts
Reģistrācijas apliecība Nr. 0221
Redakcija: Aizkraukles ielā 21, Rīga, LV-1006
Tel. 67551732, 67558694
e-pasts: ezerniec@edi.lv
Interneta adrese: www.fei-web.lv
Iespiests SIA "AstroPrint"

LATVIAN JOURNAL OF PHYSICS AND TECHNICAL SCIENCES
2016, N 4

DOI: 10.1515/lpts-2016-0023

PHYSICAL AND TECHNICAL ENERGY PROBLEMS

THE DEVELOPMENT OF NANOTECHNOLOGIES AND ADVANCED MATERIALS INDUSTRY IN SCIENCE AND ENTREPRENEURSHIP: SOCIOECONOMIC AND TECHNICAL INDICATORS. A CASE STUDY OF LATVIA (PART ONE)

I. Geipele[1], S. Geipele[1], T. Staube[1], G. Ciemleja[1], N. Zeltins[2],

[1]Institute of Civil Engineering and Real Estate Economics,
Faculty of Engineering Economics and Management,
Riga Technical University,
6-210 Kalnciema Str., LV-1048, Riga, LATVIA
E-mail: Ineta.Geipele@rtu.lv
[2]Latvian MemberKommitte of World Energy Council
21 Aizkraukles Str., LV-1006, Riga, LATVIA

The present scientific paper is the first part of two publications, where the authors obtain results from the scientific research presented in a series of works on the development of the nanotechnologies and advanced materials industry in science and entrepreneurship in Latvia. The study has a focus on finding proper socioeconomic and technical indicators. It provides resume on a scope of the study. The paper contains the developed structure of engineering economic indicator system, determined groups of indicators for assessment of the development of nanotechnologies and advanced materials industry in Latvia and results of the evaluation of the obtained statistics on the economic indicators.

Keywords: *advanced materials, development of science, economic environment level, engineering economic indicator system, nanotechnologies, research.*

1, INTRODUCTION

To ensure the effective development of the Latvian nano-field in science and entrepreneurship within the functioning institutional environment, it is necessary to perform an analysis of those indicators that characterise and/or pose a direct impact on the development of innovative material products and technological processes, as well as on the related industries and research, which are important factors for the production and commercialisation of future high technology and advanced materials according to the changes of global market and the development of technologies at present.

The **subject** of the current research is economic, social and technical indicators. The **research object** is nanotechnologies and advanced materials industry in Latvia. To reach the aim of the study – to analyse the most important indicators characterising the level of development of nano-field in quantitative terms in Latvia, the following tasks are defined: (1) to identify the importance of the engineering economic indicators determined for the development of the advanced materials field in science in Latvia; (2) to provide comparison of the economic indicators found with that of other countries if applicable; (3) to generate the data according to the levels of the economic environment; (4) to provide recommendations for business sector representatives and for the improvement of the national support programme for research and science.

The authors performed the statistical, logical, data processing and comparative analysis, studied the primary and secondary sources of the scientific literature, made a scientific overview of theoretical aspects of the issue under consideration and examined a set of indicators. To provide an overview of market data, the authors used the results of the scientific and practical study performed on the operational profile and identity of innovative multifunctional material producers in Latvia. The survey was carried out from mid-December 2014 to mid-February 2015 [1].

2. THEORETICAL FRAMEWORK AND SCIENTIFIC LITERATURE OVERVIEW

To determine technological efficiency of nanotechnology, in different countries researchers (Gholizadeh et al. 2015) use the following variables (indicators):

1) Investment (share of research and development costs of GDP, public investment in science and nanotechnology);
2) Human capital (researchers in R&D per capita; number of faculty members active in nanotechnology);
3) Technology (nanotechnology patent applications; number of nanotechnology patents per number of articles in the nano-field);
4) Industry (GDP per capita in purchasing power; GDP (purchasing power parity or ppp));
5) Science (national priorities of nanoscience; nano-articles per GDP (ppp); total number of citations of nano-articles; number of nano-articles per million people; local share of nanoscience, contribution to international cooperation in the production of nanoscience; citation index (h-index); average references per article; number of research centres in nanotechnology). However, the problem is due to the fact that data for these factors were not readily available in all countries [2].

In any field, a business activity oriented to the long term is dependent on the business environment and factors that make it up. According to the study by Dessi and Floris (2010), the economic assessment of nanotechnology business development should be carried out taking into account both the Porter five forces model, which is based on external forces, and the resource-based view (RBV), which combines the external or macro- and meso-environmental impact and the capabilities and

resources characteristic of the development of company itself or micro environment. The resource approach confirms that enterprises differ from each other in resources at their disposal, and allocation of resources among enterprises is heterogeneous, which makes a difference in business operation [3].

Exactly the use of nanotechnologies in different sectors makes it necessary to identify the factors that influence the development of the field under discussion, how the effect is manifested and which indicators can assess this impact. The RBV approach demonstrates that enterprises with a set of rare and valuable resources operate at higher efficiency. In turn, sustainable market position is associated with successful innovation activity when the introduction of new product types offsets falling profitability [4], as product and process innovations create a new value through the altered product characteristics and lower costs [5]. The company's technological innovations and operation in a free-market environment are an essential precondition for generating new ideas and satisfying consumer needs, while reducing the impact on the ecological and social environment.

Using key performance indicators (KPIs), it is possible to create a set of company's financial and non-financial indicators that may most critically affect the company's ongoing operations and future opportunities [6]. The KPIs provide management decision-making process with the information concerning the company's tactics and operating parameters in order to follow the strategy set [7], and inform what should be done to significantly improve the company's operation [6], [8]. If the KPIs are formed as a system, they lead to the changes of quantitative or qualitative results in relation to the company's strategic aim [7]. The KPIs are more frequently used in the company's corporate social responsibility programmes, including indicators and criteria related to sustainability and describing the specifics of company's operations [9]. Consequently, the basis for the company to remain competitive in the future may be considered the proper identification of KPIs [10] with the aim to focus only on the most significant indicators, deselecting all the secondary ones and reducing their number to the so-called "keys". Systematisation of information is one of the prerequisites, since the KPI choice largely depends on possibilities to identify and process the information flow so that by drawing conclusions and making decisions it could be possible to use properly prepared information, and the process would become faster and, thus, more productive. This determines the critical elements of KPI selection process: 1) the choice of indicators; 2) the intelligibility and compliance of indicators with the company's operation processes; 3) the feasibility and credibility of indicator check process [10].

3. METHODOLOGICAL SOLUTION

The developed indicator groups of engineering economic system: economic, social, technical, scientific, legal, political, ecological, health and safety, information and communication, as well as management implementation [11] have been classified by the authors according to economic environment development levels or three dimensions.

All 10 groups of indicators operate at the macro, meso and micro levels. *At the macro or global level*, there are internationally recognised indicators that are

used for national awareness and comparison of activity ratings on a global scale, and they are made available at officially recognised databases and organisation reports and/or websites. At the medium *meso or national level* of economic environment development, there are indicators that provide data for the assessment of national development promotion activities and functioning that would describe the extent of state support, as well as the public interest and activity rate for nano-industry development, including the provision of labour force and infrastructure at the local level. In turn, at the *business or micro level*, there are indicators that demonstrate the capacity of manufacturers operating in the local market for the commercialisation of nanomaterials, as well as the business capital capacity and maturity level to acquire and use new generation of nanotechnologies (see Fig. 1).

Fig. 1. Structure of engineering economic indicator system [Figure made by the authors].

According to Fig. 1, the structure of engineering economic indicator system as a solution is used for the quantitative and qualitative data analysis of each system element, as well as for the identification of universally applicable and comparable characteristics in order to establish more favourable conditions for the development of nano-field and mitigate the risks of industry problem causes.

Novelty of the study is related to the authors' comprehensive and integrated assessment approach, including economic environment development levels and identifying indicators by their belonging to the defined indicator groups for the effective determination, study, comparison and management of nano-field development to promote and develop the interaction of science and business in Latvia.

4. ASSESSMENT OF THE ECONOMIC INDICATORS

In Latvia, the nano-field develops in different industries, which have different investment parameters and quality of the labour force; therefore, the manufacture and use of innovative materials are interdisciplinary, as well as high-tech industry

volume is difficult to be identified. However, based on previous theoretical reasoning and assessment that allow identifying the most important economic, social and technical indicators of nano-field development and use, the authors have performed an in-depth analysis of these indicators at the macro, meso and micro levels and developed economic, social and technical indicator groups (see Fig. 2).

Economic Indicators

At the macro or global level, the economic indicator group includes economic development indicators that were elaborated by analysing large data arrays due to the need to universally compare the countries of the world and cover as more development areas as possible. Thus, the authors use the global innovation index (GII) and global competitiveness index (GCI) (see Fig. 2), where GII is characterised by the multi-dimensional facets of innovation, capabilities and measurable results, and this means competitiveness of a particular economy, taking into account national productivity and prosperity.

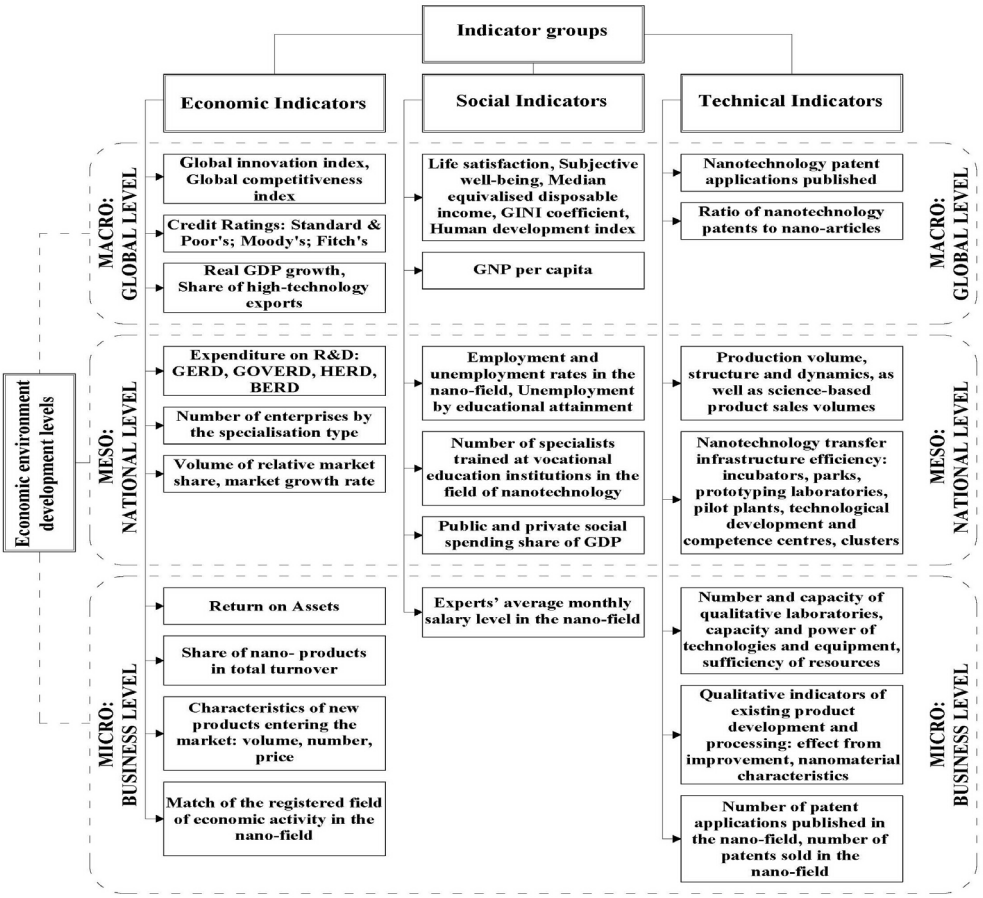

Fig. 2. Economic, social and technical indicator groups for assessment of the development of nanotechnologies and advanced materials industry [Figure made by the authors].

Out of 141 countries, Latvia took the 33rd position in the GII ranking as of 6 October 2015 with 0.77 percentage rank. In contrast, neighbouring Estonia was placed 23rd with 0.84 percentage rank, while a situation experienced by Latvia was

also characteristic of Malaysia (32nd position with 0.78 percentage rank), Cyprus and Hungary (34th position with 0.76 percentage rank and 35th position with 0.76 percentage rank, respectively). A substantial difference among the above-mentioned countries compared to Latvia is related to research and development financing from foreign funds: the highest rate is observed in Latvia (52 %), the lowest – in Malaysia (5 %); and business investment: the lowest proportion of GDP is characteristic of Latvia (22 %), the highest – of Malaysia (60 %) [12]. In relation to the GCI, out of 144 countries Latvia was ranked 42nd in the reporting period of 2014–2015, where the same value of 4.5 was reached by the Czech Republic, Azerbaijan, Mauritius, Kuwait, Lithuania, Poland, Bahrain. By contrast, neighbouring Estonia was ranked 29th in the GCI report [13]. Latvia's 42nd position is evaluated positively since in the previous report of GCI Latvia was ranked 52nd, i.e., within a year, it jumped by 10 positions. It is also important to note that this indicator can be characterised as innovation (availability of scientists and engineers; government procurement of advanced technology products; capacity of innovation), public institutions and infrastructure [14], where the evaluation of Latvia's performance is very low.

According to Fig. 2, at the macro level in the economic indicator group a significant role is played by credit rating, which is taken into account to evaluate the financial credibility of country and enterprises, which is also an important indicator to promote the development of nano-field in science and entrepreneurship in Latvia. As of 7 October 2015, Latvia's credit rating was defined as "stable outlook and upper medium grade" [15].

Compared with other European Union (EU) countries, Latvia was ranked among Slovakia (2.5 %) and Sweden (2.3 %) [16]. This demonstrates that the private consumption of households, the amount of investment provided by businesses and lending policy in Latvia do not achieve sufficient growth.

To determine the Latvian economic development trends and global challenges, the authors characterise the Latvian export structure and largest export industries in 2014, distinguishing the following product groups. The largest group is wood and wood products; charcoal (16.9 % in 2014), electrical appliances and electrical equipment (11.3 %), machinery and mechanical appliances (5.1 %), vehicles, excluding railway or tramway rolling stock, and their parts (4.1 %), iron and steel (3.6 %), iron or steel products (3.4 %) and pharmaceuticals (3.0 %) [17]. The report on the National Development Plan of Latvia until 2020 states that "in Latvia, there is a numerically small proportion of high-tech industries, which is also demonstrated by the share of high-tech products in the total exports that was 8 % in 2013", which is almost two times lower than the EU average (in 28 countries) [18]. By contrast, the share of high-tech export final value (i.e., high-tech export is less than re-export) in the foreign trade in Latvia (5.8 %) and in neighbouring Lithuania (4.8 %) is among the lowest in the world. By the highest intensity industries, the lowest profitability is demonstrated by Latvia – only 14 %, in Lithuania this indicator is 21 %. In turn, Malaysia that is compared to Latvia based on the GII ranking has reached quite a high level of 42 %, Estonia's achievement is somewhat lower – 38 %, while in Hungary – almost 50 % [12]. This analysis of export structure shows that the production of low or medium-low technology sectors dominates, and export profitability is low. Share of manufacturing industry is small in the Latvian economy, although exactly

the manufacturing industry and related service sectors play an important role in the creation of innovations and technologies. It should also be noted that not in all these sectors there is a demand for research and knowledge.

At the meso or national level, in the economic indicator group an important role is played by expenditure on R&D by sector and its financing: GERD GOVERD, HERD, BERD. In Latvia, expenditure on research activities by sector (business sector, public sector and higher education sector) and their financing accounted for only 0.68 % of GDP in 2014 [19]. For comparison purposes, in 2013 the total funding for scientific research in Latvia amounted to 0.6 % of GDP, holding approximately similar positions with Bulgaria, Cyprus and Romania. In comparison with neighbouring countries, in 2013 Lithuania's expenditure on research activities accounted for 0.95 % of GDP, but in Estonia it was 1.74 % [20]. According to the analysed data, Latvia has one of the lowest business R&D intensities in the EU as well as one of the worst criteria in Europe, i.e., expenditures on R&D. The same low evaluation of Latvia has been demonstrated by the previously analysed GCI innovation index. However, according to the data of survey carried out by the authors, only using the existing capacities, intensive growth is expected in manufacture of machinery and equipment, aviation and space industry, as well as in production of health industry, biomedicine, and biotechnology – a total of more than 7 % of the potential competence growth [1]. R&D potential, as evidenced by the willingness of local highly qualified specialists to participate in interdisciplinary and international projects, in Latvia after regaining its independence still emphasises the critical need for research development in order to promote the future growth of Latvia. GERD indicator in relation to Latvia and the comparison with other countries will be analysed under the technical indicator group at the business level, which is an important tool for the development of innovative products. Taking into account a low level of R&D growth in Latvia, the Latvian government should consider R&D potential threats as these negative R&D indicators prevent the purposeful introduction and use of modern materials in the Latvian economy. According to the report as of 8 September 2015 on achieving national development goals within the Latvian Sustainable Development Strategy until 2030 and the implementation of the Latvian National Development Plan from 2014 to 2020 [18], already in 2017 the GERD level is expected to grow at a moderate pace, reaching 1.2 % of GDP in 2017 and 1.5 % of GDP in 2020. But it is quite ambitious to plan to increase the GOVERD and HERD from the level of 0.17 % in 2012 to 0.65 % (almost four-fold increase) by 2017, and BERD – from 0.16 % in 2012 to 0.55 % of GDP in 2017. The government envisages an increase in investment activities by the private sector with the introduction of the corporate income tax relief for R&D expenses (6.^{6} Article. Expenses on Research and Development. Law "On Corporate Income Tax") [21], as well as plans the transformation of national economy in favour of production of goods and services with higher added value and will continue to attract financial instrument assets.

As the next indicator in the economic indicator group at the meso level, the authors distinguish companies by the specialisation type: the material extraction process; the type of created materials; and the used technology. The authors have studied the operation profile of innovative multifunctional material manufacturers, and according to the survey results the innovative multifunctional material manufac-

turers in Latvia mostly produce non-metal and composite products. Most respondent companies are involved in physical and chemical manufacturing. Many of them have production in both profiles. Abrasion resistance is the main type of the produced multifunctional material characteristics in Latvia. The most popular multifunctional coatings are obtained from powder – 29 % of all the respondents' answers; vacuum and deposited coatings are the second most popular type of technology used [1]. The Central Statistical Bureau of Latvia conducted its own survey of the period between 2010 and 2012, according to which the number of enterprises active in innovation accounted for 30.4 % of the total number of enterprises and the majority of them or about 65 % were large companies (more than 250 employees) [22]. More accurate data on the number of Latvian companies by various types of specialisation in the nano-field, as already mentioned in the theoretical part, are not available to the authors. The authors believe that it would be advisable to examine companies by the specialisation type in the nano-field as a study object in order to be able to identify market potential of nano-field, improve existing products and materials, as well as to prevent potential obstacles and risks in the entrepreneurship.

The same problem is attributed to the competitiveness indicators at the meso level; it is still early to forecast and determine the Latvian relative market share and market growth rate in the nano-field. As analysed above, the GCI is of major importance in determining national economic competitiveness, which is affected by many factors: institutions, infrastructure, macroeconomic environment, health and primary education, higher education and training, goods market efficiency, labour market efficiency, financial market development, technological readiness, market size, business sophistication and innovation.

At the micro or business level, the economic indicator group comprises return on assets (ROA); share of nano-products in total turnover; characteristics of new products entering the market: the volume, number, price; match of the registered field of economic activity in the nano-field. Thus, according to results of the survey performed by the authors, "only 24 % of the manufacturing companies producing innovative multifunctional materials in Latvia have specialisation in the high technology. Particular business units have reported very strong capabilities and high ROA ratio – over 25 % and around 8 %. To be successful in promotion of the manufactured nano-products, most respondents pointed to the importance of the internal factors. Most of those companies have recently had a significant increase in a market share." [1].

The remaining economic indicators at the micro level are subjectively determined characteristics, which should be assessed through targeted research, because they require the involvement of corporate competencies and commercial data analysis. The type of nano-industry production and technology use is broad, which is not distinguished and reflected by the official statistics at present. For example, according to the mentioned survey results, the analysed businesses matched the registered activity very differently. Thus, data on the field, where respondent companies operated during the survey period, showed a 33 % difference from the official register for the high technology intensity industry, i.e., the number of companies was 1.6 times higher for the production of computers, electronics and optical products [1].

Similarly, the share of nano-products in total turnover and the characteristics

of new products entering the market are usually confidential, but informative and very valuable data that would be provided by companies only for targeted research or in case of audit. By contrast, evaluating the operation of enterprises when introducing new products, the survey data demonstrated that "the highest rivalry share and more intensive growth" in Latvia could be "in manufacture of machinery and equipment, aviation and space industry, production of health industry, biomedicine, biotechnology" [1].

Taking into account the analysis of economic indicators performed at all levels, the authors conclude that the most significant impact on the company or industry's external environment is exerted by a national policy. Sustainable public administration ensures predictable manifestations in the following areas – tax and innovation policy, investment environment, and lending policy. Therefore, in these areas Latvia should adopt not only conceptual, but also action-enhancing and supporting solutions in order to promote scientific research development.

5. CONCLUSION

1. Application of nanotechnologies in various sectors with different investment parameters and quality of labour force creates a need to identify the factors that influence the development of this field, the extent of effect and the indicators that can be used to assess this impact.
2. Developing the engineering economic indicator system, the authors have supplemented and adjusted the set of indicators that reflect the development of nano-field in the context of economic, social and technical indicators. The authors have systematised indicators by economic environment development levels and compared the available analytical data in Latvia with that in other countries.
3. The authors emphasise that there is a lack of availability of data in certain economic value positions, for example: the actual enterprise specialisation and activity types for identification of nano-field relative market share, qualitative indicators of product improvement and processing or nanoproduct and technology commercialisation indicators. The authors consider that such information can be obtained from organised surveys, which can be ensured within the target projects or through involvement of the competent institutions concerned, for example, the EuroNanoForum delegates – universities, ministries of economics, European Technology Platform of Nanotechnology.
4. The use of a uniform methodology for the analysis of nano-field performance and development trends of Latvian and foreign companies on the global scale and for transnational evaluation would provide the opportunity to define more precisely the development prospects and capacities of domestic market.
5. In Latvia, the major impact on the company or industry external environment is exerted by the public policy. Sustainable public administration provides predictable manifestations in the following areas – tax and innovation policy, investment environment, and lending policy. Therefore, in these areas Latvia should adopt not only conceptual, but also action-enhancing and supporting solutions in order to promote scientific research development.

REFERENCES

1. Geipele, I., Staube, T., Ciemleja, G., Zeltins, N., & Ekmanis, J. (2015). Identity of innovative multifunctional material manufacturing business in Latvia. *Latvian Journal of Physics and Technical Sciences*, *52 (4)*, 3–18. doi: 10.1515/lpts-2015-0019
2. Gholizadeh, H., Naeini, A. B., & Moini, A. (2015). A quantitative model of technological catch-up. *International Journal of Engineering & Technology*, *4 (1)*, 233–243. doi: 10.14419/ijet.v4i1.4203
3. Dessi, C., & Floris, M. (2010). When management and customers see eye-to-eye: the agreement factor and performance. *Journal of Small Business and Enterprise Development, 17 (1)*, 102–122. doi: 10.1108/14626001011019152
4. Niessen, S., & Friedrich, R. (2009). Das Meistern der Krise für kleine und mittlere Unternehmen (KMUs): Erfolgsfaktoren und ihre Wirkung. *OnlineBlatt* 01/2009. Retrieved from http://www.malik-management.com/de/pdf/publikationen/online-letter/malik-online-letter-das-meistern-der-krise-fuer-kmus.pdf
5. Becerra, M. (2009). *Theory of the firm for strategic management economic value analysis*, Cambridge: Cambridge University Press. doi: 10.1017/CBO9780511626524
6. Parmenter, D. (2007). *Key performance indicators: Developing, implementing, and using winning KPIs*. 3rd ed. Hoboken: John Wiley & Sons.
7. Cokins, G. (2004). *Performance management: Finding the missing pieces (to close the intelligence gap)*. Chichester: John Wiley & Sons.
8. Neely, A. (Ed.). (2002). *Business performance measurement: Theory and practice*. Cambridge: Cambridge University Press.
9. Epstein, M., & Manzoni, J. (Eds.). (2006). *Performance measurement and management control improving organizations and society*. Bingley: Elsevier JAI.
10. Franceschini, F., Galetto, M., & Maisano, D. (2007). *Management by measurement: Designing key indicators and performance measurement systems*. Torino: Springer Berlin Heidelberg. doi: 10.1007/978-3-540-73212-9
11. Geipele, I., Staube, T., Ciemleja, G., Geipele, S., Zeltins, N., & Ekmanis, J. (2015). The development and design of engineering economic indicator system for nanotechnology industry product manufacturing: A case study of Latvia. *Latvian Journal of Physics and Technical Sciences, 52 (5)*, 3–19. doi: 10.1515/lpts-2015-0024.
12. The Global Innovation Index. (2015). *2015 country ranking*. Retrieved 19 October 2015, from https://www.globalinnovationindex.org/content/page/data-analysis.
13. World Economic Forum. (2014). *Competitiveness rankings*. . Retrieved 19 October 2015, from http://reports.weforum.org/global-competitiveness-report-2014-2015/rankings/
14. World Economic Forum. (2014). *Latvia in the global competitiveness report, 2014–2015.* Retrieved 19 October 2015, from http://www.nccl.lv/data/Logos/FDI%20and%20investment%20outlook_World%20Econonomic%20Forum.pdf
15. Trading economics. (n.d.).*Latvia Credit Rating*. . Retrieved 11 October, 2015, from http://www.tradingeconomics.com/latvia/rating
16. Eurostat. (n.d.). *Real GDP growth rate – Volume.* Retrieved 8 October 2015, from http://ec.europa.eu/eurostat/tgm/table.do?tab=table&init=1&language=en&pcode=tec00115&plugin=1.
17. Central Statistical Bureau of Latvia. (n.d.). *Latvia's foreign trade. Main commodities and partners in 2014.* Retrieved 8 January 2016, from http://www.csb.gov.lv/sites/default/files/nr_28_areja_tirdznieciba_preces-partneri_14_04_lv.pdf (in Latvian).

18. National Development Plan of Latvia's Portal (2015). *The prime minister will report on achieving the national development objectives and implementation of the NAP2020*. Retrieved 5 January 2016, from: http://www.pkc.gov.lv/443-inistru-prezidente-zi%C5%86os-par-valsts-att%C4%ABst%C4%ABbas-m%C4%93r%C4%B7u-sasnieg%C5%A1anu-un-nap2020-%C4%ABsteno%C5%A1anu (in Latvian).
19. Central Statistical Bureau of Latvia. (n.d.). *Expenditure on research activities by sector and their financing (mln. EUR)* Retrieved 5 January 2016, from http://data.csb.gov.lv/pxweb/lv/zin/zin__zin/ZI0030_euro.px/table/tableViewLayout1/?rxid=ce8a-ac91-f2b0-4f13-a25d-29f57b1468fb (in Latvian).
20. Eurostat statistics explained. (n.d.). *Europe 2020* indicators – Research and development. Retrieved 15 November 2015, from http://ec.europa.eu/eurostat/statistics-explained/index.php/Europe_2020_indicators_-_research_and_development.
21. LR Legislation. (2015). *Law on Corporate Income Tax*. Retrieved 9 January 2016, from http://likumi.lv/doc.php?id=34094 (in Latvian).
22. Central Statistical Bureau of Latvia. (n.d.). *Informative survey "Innovation in Latvia for 2010–2012"*.. Retrieved 15 November 2015, from http://www.csb.gov.lv/sites/default/files/nr_37_inovacijas_latvija_14_00_lv.pdf (in Latvian).

NANOTEHNOLOĢIJU UN VIEDO MATERIĀLU INDUSTRIJAS ATTĪSTĪBA ZINĀTNES UN UZŅĒMĒJDARBĪBAS JOMĀS: SOCIĀLEKONOMISKIE UN TEHNISKIE RĀDĪTĀJI. LATVIJAS PIEREDZE (PIRMĀ DAĻA)

I. Geipele, S. Geipele, T. Štaube, G. Ciemleja, N. Zeltiņš,

Kopsavilkums

Dotais zinātniskais raksts ir viens no divām ieplānotajām publikācijām, kurās autori apkopo zinātniskā pētījuma gaitā iegūtos rezultātus. Šis darbs ir zinātnisko rakstu sērijas turpinājums, veltīts nanotehnoloģiju un viedo materiālu industrijas attīstības līmeņa noteikšanai un paaugstināšanai zinātnē un uzņēmējdarbības jomā Latvijā. Pētījumam autori ir uzstādījuši mērķi noskaidrot īpaši nozīmīgos sociālekonomiskos un tehniskos rādītājus. Šādi, šis raksts sniedz apkopojumu par pētījuma diapazonu, kā arī ietver sevī izstrādāto inženierekonomisko rādītāju sistēmas struktūru, rādītāju grupas nanotehnoloģiju un viedo materiālu industrijas attīstības noteikšanai Latvijā un statistisko datu izvērtējuma rezultātus par ekonomiskajiem rādītājiem.

07.03.2016.

LATVIAN JOURNAL OF PHYSICS AND TECHNICAL SCIENCES
2016, N 4

DOI: 10.1515/lpts-2016-0024

INTERLEAVED DC-DC CONVERTER WITH DISCRETE DUTY CYCLE AND OPEN LOOP CONTROL

K. Kroics[1], A. Sokolovs[2]

[1]Institute of Physical Energetics
21 Aizkraukles Str., Riga, LV 1006, LATVIA
e-mail: kaselt@inbox.lv
[2]Riga Technical University Cesis Branch
3 Piebalgas Str., Cesis, LV-4101, LATVIA
e-mail: alvis.sokolovs@rtu.lv

The authors present the control principle of the multiphase interleaved DC-DC converter that can be used to vastly reduce output current ripple of the converter. The control algorithm can be easily implemented by using microcontroller without current loop in each phase. The converter works in discontinuous conduction mode (DCM) but close to boundary conduction mode (BCM). The DC-DC converter with such a control algorithm is useful in applications that do not require precise current adjustment. The prototype of the converter has been built. The experimental results of the current ripple are presented in the paper.

Keywords: *DC-DC power converters, discontinuous conduction mode multiphase switching converters.*

1. INTRODUCTION

Interleaving control schemes of the DC-DC converters are more often used in the converter applications, especially in the converters that require high power capability and high performance. Benefits of such control methods include reduction of size, losses and cost of the input and output filters, reduction of current stress of the dc bus capacitor, improved dynamic performance and increase in the power capacity of the converters. Interleaved DC-DC converters are used in various applications: as voltage regulation modules [1]–[2], renewable applications [3]–[5], traction applications [6]–[8] and in other areas.

The current of the interleaved DC-DC converter can be controlled in the two modes: continuous conduction mode (CCM) or DCM. When the converter operates in the DCM, zero current switching can be implemented without additional control or components; smaller inductance than in the CCM is necessary. In the discontinuous conduction mode (DCM), the reverse-recovery losses of the diode are eliminated

and switching losses can be reduced. On the other hand, input current and output voltage ripple are increased in the DCM. Due to this reason, it is important to find a way how to reduce this ripple. Moreover, most of the published papers require a current control loop in each phase to achieve balanced phase currents and to improve transients [9]–[12]. The cost, weight and control complexity grow when the number of phases increases due to the control loop into each phase; therefore, open-loop control allows solving this problem.

The particular control method of the DC-DC converter can not provide accurate regulation of the current but in many applications it is not necessary. One of the examples is the boost or buck-boost converter in a DC drive (Fig. 1.). As a DC motor has a very high starting current that has the potential of damaging the internal circuit of the armature winding, current must restricted to some limited value. Therefore, all DC motors must be provided with a means to limit the starting current to reasonable values. Thus, during transition processes and when high torque is required the proposed control method is applicable, but when low current is required then the DC-DC converter can work in deeper DCM mode or a number of the active phases can be reduced.

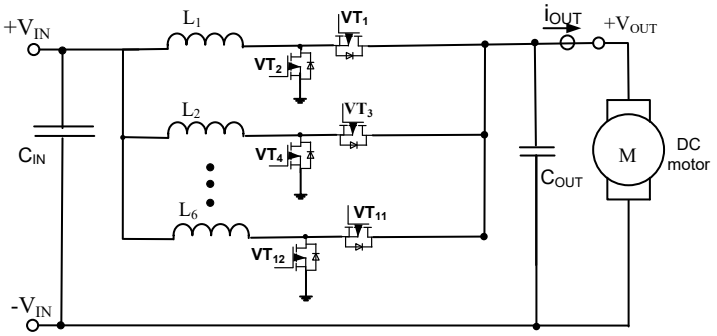

Fig. 1. Six-phase boost converter for DC drive.

The proposed control method uses variable frequency mode. Compared to DCM with constant switching frequency [12], [13], [14], [15] variable frequency mode yields to lower total harmonic distortion of the current and smaller peak inductor currents and results in lower switching and conduction losses. As the MOSFETs (metal–oxide–semiconductor field-effect transistors) have parasitic capacitance and the converter works close to boundary conduction mode, it is possible to achieve zero voltage switching conditions similar as in [16], [17], [18].

2. THE CONTROL METHOD

The operation into the DCM requires a phase ripple current larger than twice the average phase current. Therefore, the use of a large output capacitance is necessary to hold a constant output voltage. But as in a multiphase converter, the phases share current equally and the phase ripple is proportional to the current that flows in each phase, the phase ripple decreases if the number of phases increases. Even more depending on the duty cycle, the actual output ripple can be lower due to ripple cancelation between the phases:

$$\Delta i_o = \frac{V_{IN}}{f_{sw} L N^2}\left[\left(Nm - floor(Nm)\right) - (Nm - floor(Nm))^2\right] \text{ [19]}, \quad (1)$$

where V_{IN} – input voltage; f_{sw} – switching frequency; L – inductance; N – number of phases; m – modulation index.

By using (1), it is possible to draw curves shown in Fig. 2. As can be seen from Fig. 2, the current ripple reaches zero when the modulation index is equal to multiple of 1/N. In a particular six-phase case, the zero current ripple takes place by duty cycle equal to 0.17, 0.33, 0.50, 0.67 and 0.83. Of course, in real design exactly zero current ripple is hard to reach due parasitic resistance, capacitance, inductance and transients into circuit. The six-phase converter has less than 0.8 percent output ripple by any duty cycle.

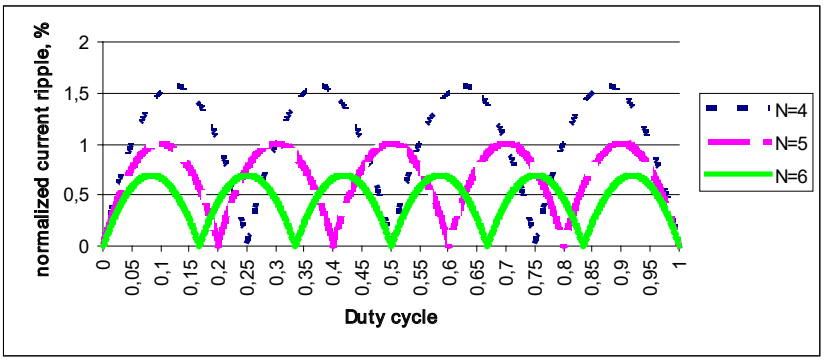

Fig. 2. Normalized output current ripple of boost converter.

One of the problems that must be considered in the design of the interleaved converter is current sharing. One of the solutions is to include an additional current loop. This leads to higher cost, increased size and decreased reliability of the converter. The goal of the paper is to use a large number of phases but without any current loop in each phase. In continuous conduction mode (CCM), a 1% difference in one duty cycle causes a 47% unbalance in the current of the unbalanced phase [15]. Misbalance of the currents is also caused by unequal inductance and parasitic resistance. In the discontinuous conduction mode (DCM), equalization of the currents is much better. In the DCM, the differences in phase current are caused by duty cycle, inductance and not parasitic resistance. Since each phase current starts from zero every switching cycle, the average values are quite similar even if the duty cycles are relatively different.

In the DCM mode, per-phase current is determined in each period and it does not depend on the previous periods. This greatly improves the converter dynamics and simplifies control system of the converter as if any converter is stable in the CCM, then it will be stable in the DCM as well.

In the boundary conduction mode (BCM), the peak current in the inductor (Fig. 3.) is twice the average current. Therefore, this mode is the most economical and control will be designed to ensure work of the converter in the DCM mode as

close as possible to the BCM. The summary output current I_{out} of n phase converter is the sum of all choke currents. In the BCM, the peak current in the choke (I_m) can be expressed as shown below:

$$I_m = \frac{2 \cdot I_{IN}}{N}. \tag{2}$$

Using the inductance (L) as well as the input (V_{in}) and output (V_{out}) voltage, the required on-time (t_{on}) and off-time (t_{off}) for boost mode can be calculated as shown in (4) and (5) and similarly for boost mode to ensure operation in boundary conduction mode:

$$t_{ON} = I_m \frac{L}{V_{out}}, \tag{3}$$

$$t_{OFF} = I_m \frac{L}{V_{in} - V_{out}}. \tag{4}$$

As the DC-DC converter works at a constant duty cycle (D), the switching period (T) can be calculated as follows:

$$T = \frac{t_{ON}}{D}. \tag{5}$$

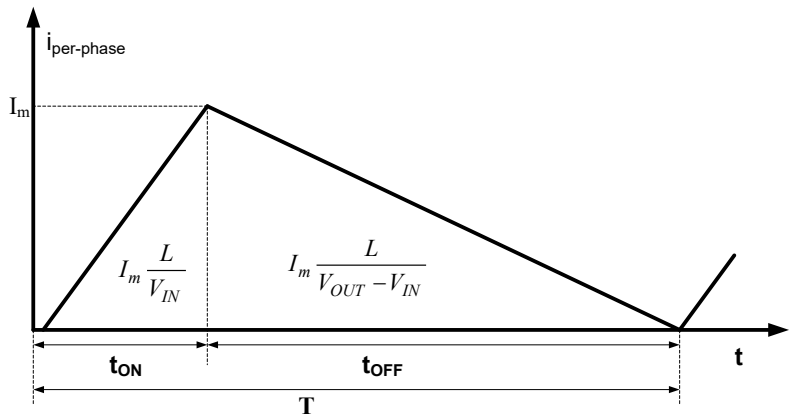

Fig. 3. Inductor current in boundary conduction mode within boost mode.

The selection of the duty cycle D may be carried out in several ways. The simplest method is to control output voltage by discrete values. If the converter has a large number of phases, then in such a way output voltage with normal resolution can be formed.

Figure 4 shows the method of controlling current during starting of the motor with the boost converter. The method is a bit similar to the use of starting resistors only without energy losses. The main principle is to control input current (I in Fig. 4), and if current decreases to some minimum value then transition to the next duty

cycle takes place. The variable I_m can be calculated by (2), if input current I_{IN} is measured by current sensor. By using (3) and (5) time and period values can be calculated. The converter works in variable frequency mode close to the BCM.

If no current regulation is necessary after the starting process, the converter can work at a constant duty cycle to ensure nominal output voltage. If current control is required, then the converter can work at any duty cycle. Although current ripple will be relatively larger, it will not be so important because the nominal current is much smaller than starting current; therefore, current ripple will be lower anyway.

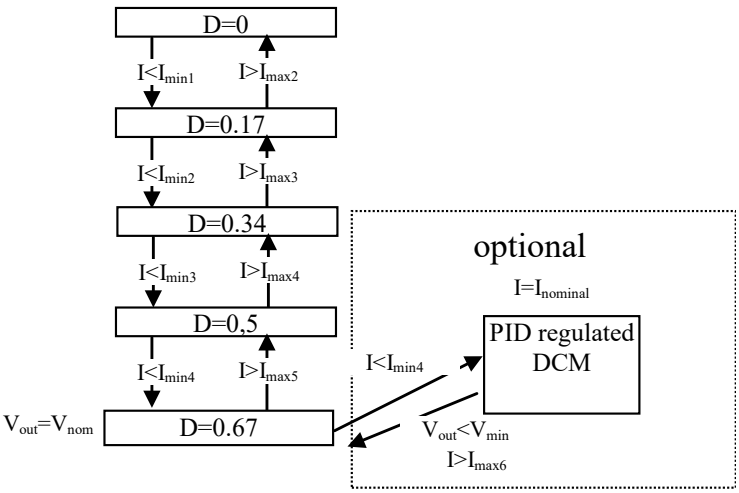

Fig. 4. Duty cycle changing algorithm of boost converter during starting of the motor.

One of the methods of current control is that the variable I_m can be used not only to maintain the desirable current, and t_{on} and t_{off} are calculated by equations (3) and (4). This can be done if I_m is output of the proportional-integral (PI) regulator. This method is described in [4]. Another method is working with constant switching frequency in the DCM. Some control algorithms in this mode are discussed in [12], [14], [15]. Also work in the CCM is possible. It can be done if some phases work in parallel mode and additional current sensors are placed in these branches. Many other control methods can be implemented, too.

3. RESULTS AND DISCUSSION

Figure 5 shows the prototype of the six-phase boost converter. In the figure, 1 denotes power supply for driver circuits, 2 is the digital signal processor that provides control of the converter, 3 – inductors, 4 – MOSFET transistors. The inductors used in this interleaved converter have a low inductance value as the converter works in the DCM. The inductance of the inductor is equal to 50 μH; it consists of 5 windings of Litz wire on the RM8 core, the ceramic capacitors are placed near the transistors to reduce the impact of parasitic inductance. PSMN6R5-80BS MOSFET transistors and STM32F407 digital signal processor are used in the prototype.

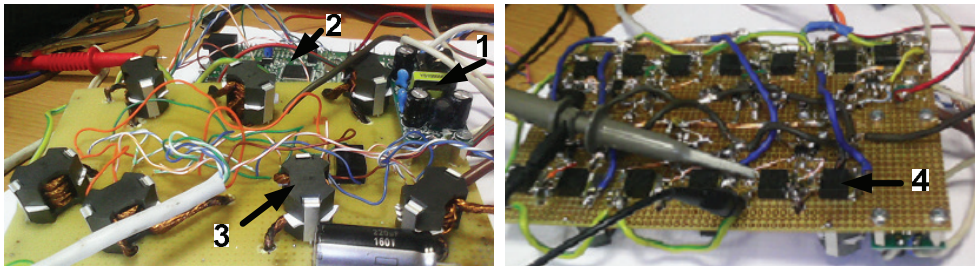

Fig. 5. The prototype of the boost converter.

Figure 6 shows per-phase current of DC-DC converter in the DCM. As can be seen, current goes a little into the negative, it means that zero voltage switching can be achieved in the BCM because the inductor current declines under zero and a subsequent oscillation between inductor and parasitic MOSFET capacitors starts in which the voltage over MOSFET drops to zero (or near zero).

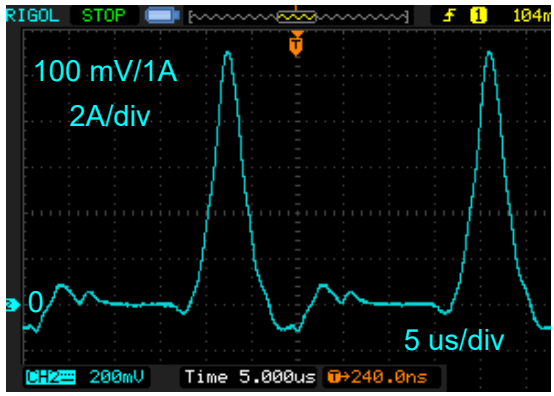

Fig. 6. Per-phase current in the DCM.

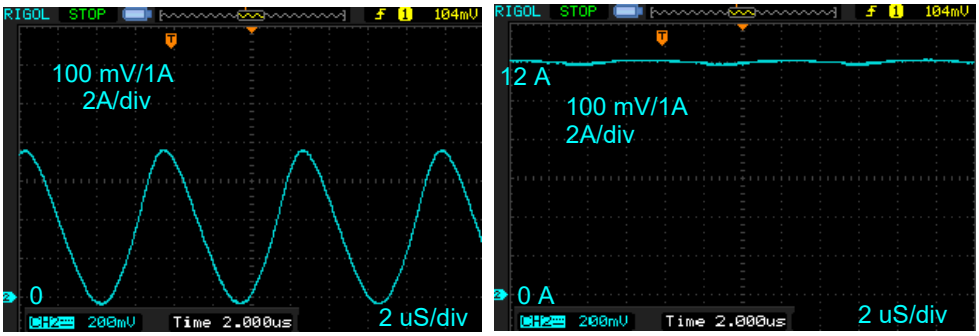

Fig. 7. Per-phase current and input current of the interleaved DC-DC boost converter.

Figure 7 shows per-phase and output current of the boost converter in the BCM. The switching frequency of the converter in the experiment was close to 170 kHz. As current probe with the bandwidth of 200 kHz is not available, current has a bit filtered shape. The algorithm described above allows correctly calculating the period to ensure work in the BCM.

4. CONCLUSIONS

In this paper, the control algorithm of interleaved multiphase DC-DC converter has been described. The converter with such an algorithm can be designed avoiding the use of current loops that would not be feasible with a very large number of phases. The algorithm can be used in many applications. In the paper, the application example has been shown for motor starting with the boost converter. The converter works at discrete duty cycles that allow reducing output and input current ripples and size of capacitors. Operation in the BCM allows implementing zero voltage and zero current switching without additional elements. The algorithm can be implemented using digital control. The experimental prototype has been developed, and experimental results have been shown. The further research is needed to investigate the change of active number of phases to increase operating points with tiny current ripple.

REFERENCES

1. Wong, P.-L., Xu, P., Yang, B., and Lee, F.C. (2001). Performance improvements of interleaving VRMs with coupling inductors, *IEEE Transactions on Power Electronics 16* (4), 499–507.
2. Panov, Y., and Jovanovic, M.M. (2000). Design considerations for 12-V/1.5-V, 50-A voltage regulator modules. In *Proceedings of Applied Power Electronics Conference and Exposition* (pp. 39–46).
3. Kroics, K., Sirmelis, U., Grigans, L., and Brazis, V. (2015). Digitally controlled 4-phase interleaved DC-DC converter with coupled inductors for storage application in microgrid. In *Proceedings of 9th International Conference Compatibility and Power Electronics* (pp. 504–509).
4. Kroics, K. (2015). Bi-directional two level 6-phase DC-DC converter for energy storage application. In *Proceedings of Conference for Power Electronics, Intelligent Motion, Renewable Energy and Energy Management (PCIM Europe)* (pp. 1–8).
5. Shen, J., Rigbers, K., and De Doncker, R.W. (2010). A novel phase-interleaving algorithm for multiterminal systems. *IEEE Transactions on Power Electronics 25* (3), 741–750.
6. Shrud, A., Bonsbaine, A., Ashur A.S., Thorn, R., and Benmusa, T. (2009). Modeling and simulation of automotive interleaved buck converter. In *Universities Power Engineering Conference (UPEC)* (pp. 1–6).
7. Jen, C., Li, J., and Sullivan, R. (2003). Automotive application of multi-phase coupled-inductor DC-DC converter. In *IEEE Industry Applications Conference* (pp. 1524–1529).
8. Hirakawa, M., Watanabe, Y., Nagano, M., Andoh, K., Nakatomi, S., Hashino, S., and Shimizu, T. (2010). High power DC/DC converter using extreme close-coupled inductors aimed for electric vehicles. In *Power Electronics Conference IPEC 2010* (pp. 2941–2948), Singapore.
9. Qahouq, A. (2009). N-phase efficiency-based current sensing auto-tuning controller. In *Proceedings of Appl. Power Electron. Conf. (APEC)* (pp. 274–279).
10. Min, B.S., Park N.J., and Hyun, D.-S. (2007). A novel current sharing technique for interleaved boost converter. *Proceedings of Power Electronics Specialist Conference (PESC)* (pp. 2658–2663).

11. Zhou, X., Xu P., and Lee, F. C. A novel current-sharing control technique for low-voltage high-current voltage regulator module applications. *IEEE Transactions on Power Electronics 15* (6), 1153–1162.
12. Nandankar, P., and Aware, M.V. (2012). High efficiency discontinuous mode interleaved multiphase bidirectional dc-dc converter. In *Power Electronics*, *Proceedings of Drives and Energy Systems conference (PEDES)* (pp. 16–19).
13. Zakis, J., Vinnikov, D., Roasto, I., and Ribickis, L. (2011). Quasi-Z-source inverter based bi-directional DC/DC converter: Analysis of experimental results. In *Proceedings of Compatibility and Power Electronics Conference* (pp. 394–399).
14. Liqin, N., Patterson, D.J., and Hudgins, J.L. (2012). High power current sensorless bi-directional 16-phase interleaved DC-DC converter for hybrid vehicle application. *IEEE Transactions on Power Electronics 27* (3), 1141–1151.
15. Garcia, O., Zumel, P., Castro, A., Cobos, J.A., and Uceda, J. (2004). An automotive 16 phases DC-DC converter. In *Proceedings of Power Electronics Specialists Conference* (pp. 350–355).
16. Vazquez, A., Rodriguez, A., Martin, K., Arias, M., and Hernando, M.M. (2013) Inductor optimization for multiphase interleaved synchronous bidirectional boost converter working in discontinuous conduction mode with zero voltage switching. In *Proceedings of Energy Conversion Congress and Exposition (ECCE)* (pp. 4977–4984).
17. Zakis, J., Vinnikov, D., and Roasto, I. (2010). Soft-switching capability analysis of a qZSI-based DC/DC converter. In *Proceedings of 12th Biennial Baltics Electronics Conference* (pp. 301–304).
18. Shuqiu, G., Ming, Y., Xiying, D., and Bin, H. (2008). Research of interleaved three-phase bidirectional DC/DC converter based on control type soft switching. In *Proceedings of International Conference on Electrical Machines and Systems* (pp. 1738–1741).
19. Grbovic, P.J. (2013). Closed form analysis of N-cell interleaved two-level DC-DC converters: The DC bus capacitor current stress. In *Proceedings of the ECCE Asia Downunder* (pp. 122–129).

VAIRĀKFĀŽU LĪDZSTRĀVAS PĀRVEIDOTĀJS AR DISKRĒTU AIZPILDĪJUMU UN BEZ ATGRIEZENISKĀS SAITES

K. Kroičs, A. Sokolovs

K o p s a v i l k u m s

Rakstā piedāvāts izmantot līdzstrāvas pārveidotāju, mainot aizpildījumu diskrēti - tas ir, izvēloties tādas vērtības, pie kurām strāvas pulsācijas ir minimālas. Šāds risinājums ļauj samazināt pārveidotāja izmērus un izmaksas, kā arī ir iespējams realizēt bezsprieguma un bezstrāvas komutāciju. Pārveidotājs var tikt izmantots risinājumos, kur ir pieļaujama diskrētas formas sprieguma izmantošana vai arī neprecīzai strāvas regulēšanai. Kā piemērs apskatīts paaugstinošā līdzstrāvas impulsregulatora izmantošana motora startēšanai. Piedāvātā metode var tikt realizēta, izmantojot mikrokotroleri. Rakstā aprakstīts prototips, kura darbības pamatā ir pielietotā metode.

02.06.2016.

LATVIAN JOURNAL OF PHYSICS AND TECHNICAL SCIENCES
2016, N 4

DOI: 10.1515/lpts-2016-0025

STUDY OF THE SYNCHRONOUS RELUCTANCE MOTOR DESIGN

J. Dirba, L. Lavrinovicha, R. Dobriyan

Riga Technical University,
12/1 Azenes Str., Riga, LV-1048, LATVIA
e-mail: janis.dirba@rtu.lv

The paper focuses on studying the external-rotor synchronous reluctance motor. The analysis is performed to estimate the influence of the number of stator slots and non-magnetic areas in the rotor (i.e., flux barriers) on the electromagnetic torque and torque ripple of the studied motor. It is concluded that the increase in the number of stator slots $Z = 6$ to $Z = 18$ causes an approximately twofold decrease in the ripple factor, but torque increases by 5 %. Electromagnetic torque will be increased approximately by 24 %, if non-magnetic flux barriers are created in the rotor of the studied synchronous reluctance motor.

Keywords: *electromagnetic torque, number of the stator slots, synchronous reluctance motor, torque ripple.*

1. INTRODUCTION

The brushless synchronous motors (permanent-magnet synchronous motors and synchronous reluctance motors) are considered a good alternative to brushed motors, because they have a significantly high level of safety and other advantages [1]–[4].

Permanent-magnet synchronous motors have such disadvantages as high cost of permanent magnets and high electromagnetic torque ripple. High electromagnetic torque ripple of such motors is the result of the cogging torque that is due to the interaction between permanent magnets of the rotor and the stator slots. Synchronous reluctance motors in comparison with permanent-magnet synchronous motors have low value of the electromagnetic power (torque) per unit volume. Moreover, synchronous reluctance motors have high electromagnetic torque ripple that is the result of the rotor magnetic asymmetry.

Synchronous reluctance motors (SynRMs) have neither winding of excitation nor permanent magnets, which is why they are safer and cheaper in comparison with other types of electric motor. SynRM operation principle is based on a deep variation in the magnetic flux due to different reluctance on its way.

Opportunities of SynRM strongly depend on the structural features of the rotor. The stator of such a motor can be the same as the stator of induction motor, while the rotor is safer and its design is simpler [5]. To increase the value of electromagnetic torque per unit volume of SynRM, the segmental rotor design is proposed. This rotor has ferromagnetic segments separated to each other by non-magnetic gap [6]. However, the influence of the stator slot number and other structural parameters on the motor performance has not been studied in detail.

Questions of the electromagnetic torque ripple reduction are discussed in many papers from different points of view [1]–[3]. Two most common techniques for electromagnetic torque ripple reduction are shortening of stator winding pitch and stator slot skewing [1]. However, slot skewing in synchronous reluctance motors is not an effective technique because, firstly, it does not fully prevent torque ripple and, secondly, it significantly reduces motor torque [2]. Furthermore, in such a case, copper losses will be greater, and winding automatic creation will be quite complicated due longer stator winding.

The main goal of the paper is to study the influence of stator slot number and non-magnetic flux barriers on the electromagnetic torque ripple of SynRM.

2. PROTOTYPE OF SYNCHRONOUS RELUCTANCE MOTOR

A two-pole three-phase synchronous reluctance motor having external segmental rotor is selected as an object of the research [6]. Figure 1 presents a cross-section of the motor under investigation, which has a six-slot stator. There are different cases provided for studding, when a number of stator slots: Z=6, Z=12, Z=18 and Z=24. Outer diameter of the motor is assumed to be a constant value. The rotor of the motor is made of special segmental cores that are composed of electrical steel sheets. In order to decrease the influence of the quadrature magnetic field on the motor operation, segmental rotor is made with additional non-magnetic areas (i.e., flux barriers) in the middle of each segment along the quadrature axis. Holes in the rotor segmental cores (Fig.1) are made for rotor placement in the motor body by stud-bolts.

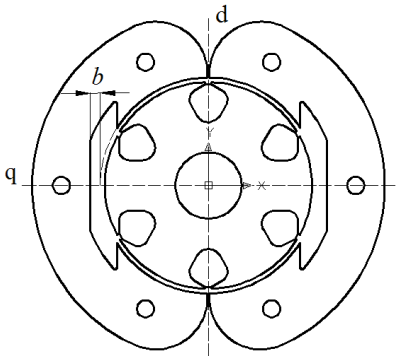

Fig.1. A cross-section of the prototype.

Width of the additional non-magnetic flux barriers (width b in Fig. 1) is assumed to be a variable value to study its influence on the electromagnetic torque.

3. STUDIED MOTOR MAGNETIC FIELD SIMULATION AND RESULT ANALYSIS

In order to evaluate possibilities of reducing electromagnetic torque ripple of the studied motor and at the same time ensuring the high value of torque, the magnetic field of studied SynRM is simulated by the finite element method. In this case, electromagnetic torque of the studied motor is calculated using the Maxwell stress tensor [7]. In this case, the electromagnetic torque is described with surface integral (1) over a closed surface S in the middle of the motor air gap.

$$T_{\varepsilon\mu} = \oint_{\Sigma}\left(\bar{\rho} \cdot \left[\frac{1}{2\mu_0}\left(B_{\nu}^2 - B_{\tau}^2\right) \cdot \bar{\nu} - \frac{1}{\mu_0} B_{\nu} B_{\tau} \bar{\tau} \right] \right) \delta\Sigma , \quad (1)$$

where T_{em} is the electromagnetic torque;

μ_0 is vacuum magnetic permeability;

$\bar{n}$ is the normal vector of the point on a closed surface *S*;

$\bar{r}$ is the radius-vector of the point on a closed surface *S*;

$\bar{t}$ is the tangent vector of the point on a closed surface *S*;

B_n is the normal component of the magnetic flux density;

B_t is the tangential component of the magnetic flux density.

Electromagnetic torque ripple of brushless synchronous motor strongly depends on the number of stator slots and their opening width [8]. Therefore, firstly, the influence of the number of stator slots on the torque ripple is studied in the present research.

Figure 2 shows electromagnetic torque curves depending on the rotation angle of the rotor obtained by magnetostatic simulation of studied SynRM in the cases when $Z = 6$, $Z = 12$, $Z = 18$ and $Z = 24$.

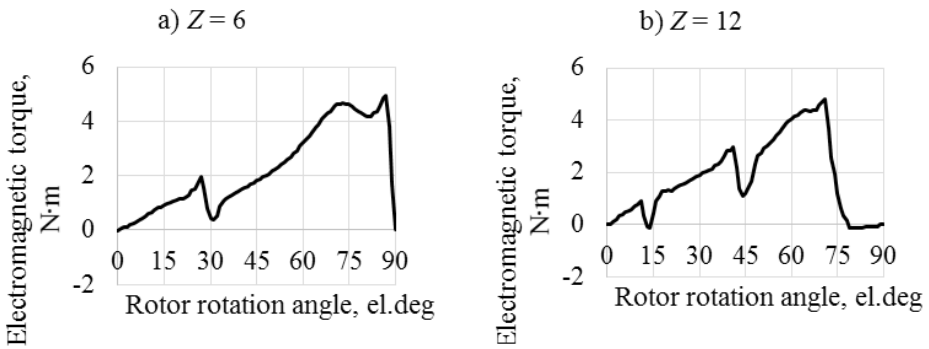

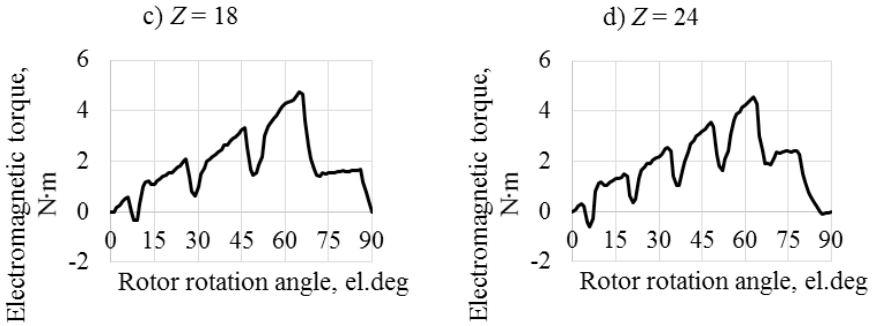

Fig. 2. Electromagnetic torque curves depending on the rotation angle of the rotor at different number of stator slots.

As it is known [9] from (2), electromagnetic torque of synchronous motor with unsaturated magnetic circuit depending on the angle ε between the rotor direct axis and axis of armature magnetizing force has sinusoidal change.

$$T_{em} = \frac{1}{2} mpL_{ad} I_1^2 \left(1 - \frac{k_q}{k_d}\right) \sin(2\varepsilon), \tag{2}$$

where m is the number of phases;

p is the number of pole pairs;

L_{ad} is the inductance corresponding to the armature magnetic flux along the direct axis;

I_1 is the armature current;

k_q is the armature reaction factor along the quadrature axis;

k_d is the armature reaction factor along the direct axis.

Therefore, it is useful to excrete the fundamental harmonic T_{em1} from curves presented in Fig. 2. Thus, torque ripple can be evaluated by the proposed coefficient k_p, which can be termed as a ripple factor:

$$\kappa_\pi = \frac{\sum_{i=1}^{\nu} |\Delta\alpha|}{\nu \cdot \mathrm{T}_{\mu\alpha\xi 1}}, \tag{3}$$

where n is the number of evenly selected points on the half interval of the electromagnetic torque sinusoidal curve;

Δa is the difference between values of the electromagnetic torque T_{em} and the fundamental harmonic of electromagnetic torque T_{em1} in relevant points;

T_{max1} is the maximum of electromagnetic torque fundamental harmonic.

Relationships $k_p = f(n)$ for a different number of stator slots are shown in Fig. 3. From these curves it can be concluded that the selected number of points $n \geq 45$ guarantees sufficiently safe notification of ripple factor k_p.

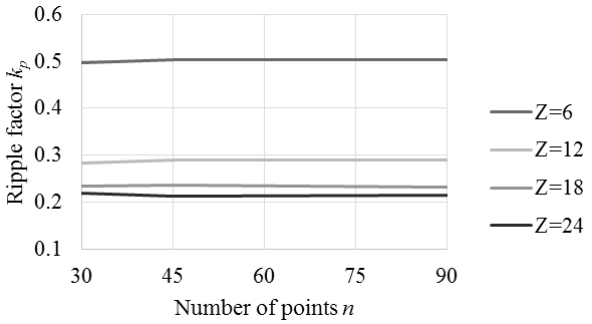

Fig. 3. Relationships $k_p = f(n)$ for different cases with the studied number of stator slots.

Figure 4 demonstrates variation of torque T_{max1} and ripple factor k_p depending on the number of stator slots. Those values are defined from results of prototype magnetic field calculations by (1) and (3).

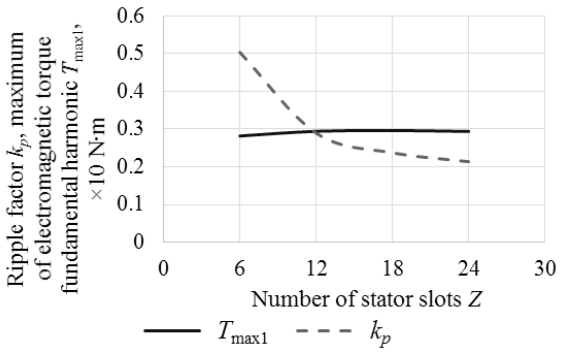

Fig. 4. Variation of torque T_{max1} and ripple factor k_p depending on the number of stator slots.

Curves in Fig. 4 show that if the number of stator slots increases, ripple factor k_p significantly reduces; however, the change of maximum value of the torque fundamental harmonic T_{max1} is minor. Thus, the number of stator slots $Z = 18$ is the most acceptable variant because, taking into account mechanical strength of stator teeth and stator winding creation, too large number of stator slots is not desirable.

In order to clarify results of additional non-magnetic flux barrier influence on the T_{max1} and k_p values, some calculations are made by changing width b. Figure 5 presents relationships $T_{max1} = f(b)$ and $k_p = f(b)$ for the studied motor having $Z = 18$.

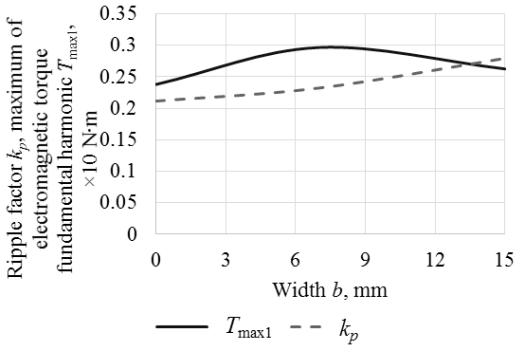

Fig. 5. Torque T_{max1} and ripple factor k_p versus width of the non-magnetic flux barrier.

From curves in Fig. 5 it can be concluded that the increase of width b in the beginning causes the increase of torque T_{max1} due to the increase of magnetic asymmetry of the rotor; then torque T_{max1} reduces due to a significant increase of magnetic circuit saturation. However, the influence of flux barrier width b on the ripple factor k_p is not significant.

4. RESULTS OF EXPERIMENTAL TESTING OF THE STUDIED MOTOR AT BRAKE ROTOR

Angular curves of a synchronous motor can be determined experimentally in the static mode by powering the armature winding with a certain value of DC current. In this case, the rotor is breaking by constant magnetizing force [9].

According to the method for determination of static electromagnetic torque, the fundamental harmonic of magnetizing force generated by DC current at a brake rotor is to be equal to that generated by AC current in the case of rotation rotor.

In order to perform experimental testing, the external-rotor motor is mounted on a fixed static shaft. Structural scheme of experimental stand for determination of angular curves for external-rotor motors is shown in Fig. 6.

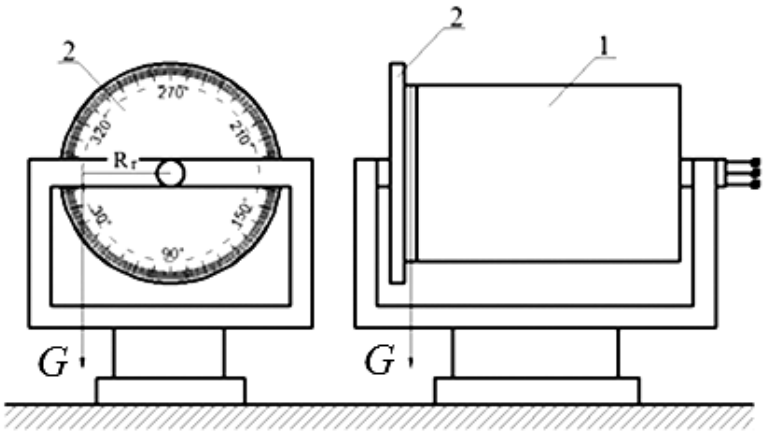

Fig. 6. Structural scheme of experimental testing stand for external-rotor motor: 1 – studied motor; 2 – graduated disc for determination of rotor rotation angle; G – suspended weight to the rotor.

Experimental testing results are compared with results obtained by magnetostatic field simulation of the studied motor. Magnetostatic field simulation is made with two-dimensional software QuickField [10]. Figure 7 presents experimentally obtained angular curves of the studied prototype with $Z = 6$ in comparison with calculated curves obtained by magnetostatic field simulation. Evaluated results show a satisfactory coincidence of experimental and numerically calculated results.

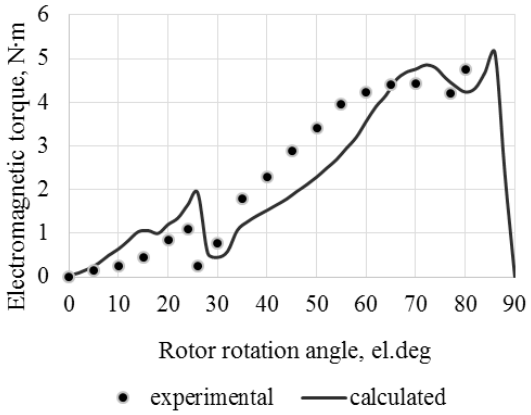

Fig. 7. Experimentally obtained and numerically calculated angular curves of the studied prototype.

5. CONCLUSIONS

Based on the results obtained, the following conclusions can be drawn:

1. Ripple factor, which is calculated as the average amount of deviation from the fundamental harmonic of electromagnetic torque curve, can be used for ripple evaluation for synchronous motor.
2. Ripple factor is substantially reduced by increasing the number of stator slots; however, the increase of the torque fundamental harmonic maximum is not significant. Therefore, the increase of the number of stator slots $Z = 6$ to $Z = 18$ causes an approximately twofold decrease of the ripple factor, but torque increases by 5 %.
3. Electromagnetic torque will be increased approximately by 24 %, if non-magnetic flux barriers are created in the rotor of the studied synchronous reluctance motor.

ACKNOWLEDGEMENTS

The present research has been supported by the State Research Programme "LATENERGI".

REFERENCES

1. Wang, K., Zhu, Z.Q., Ombach, G., Koch, M., Zhang, S., and Xu, J. (2015). Torque ripple reduction of synchronous reluctance machines: Using asymmetric flux-barrier. *International Journal of Computations and Mathematics in Electrical and Electronic Engineering 34* (1): 18-31 DOI: 10.1108/COMPEL-11-2013-0367.
2. Fratta, A., Troglia, G.P., Vagati, A., and Villata, F. (1993). Evaluation of torque ripple in high performance synchronous reluctance machines. In *Conf. Rec. IEEE IAS Annu. Meeting* (pp. 163–170). Ontario, Canada.

3. Vagati, A., Pastorelli, M., Franceschini, G., and Petrache, S.C. (1998). Design of low-torque-ripple synchronous reluctance motors. *IEEE Transactions on Industry Applications 34* (4).
4. Dirba, J., Lavrinovicha, L., and Dobriyan, R. (2015). The prospects of synchronous reluctance motors usage in low power electrical devices. *Latvian Journal of Physics and Technical Sciences 52* (2), 40–48. ISSN 0868-8257.
5. Lipo, T.A. (1991). Synchronous reluctance machines – A viable alternative for AC drives. *Electric Machines and Power Systems*, 659–671.
6. Pugachevs, V., Dirba, J., Kukjane, L., Levins, N., and Orlova, S. (2012). Patent of the Republic of Latvia. LV 14418 B. (in Latvian).
7. Bianchi, N. (2005). *Electrical machine analysis using finite elements.* CRC Press, Boca Raton, FL, Taylor & Francis.
8. Nizam, M., Waloyo, H.T., Inayati. (2013). Design of optimal outer rotor brushless DC motor for minimum cogging torque. In *Joint International Conference on Rural Information & Communication Technology and Electric-Vehicle Technology* (pp. 1–4).
9. Lavrinovicha, L. (2014). *Design and optimisation of brushless synchronous motors for use in low power equipment*. Summary of PhD Thesis. Riga: RTU.
10. Tera Analysis (2010). *QuickField. Finite Element Analysis System. Version 5.7.* User's Guide (Denmark).

SINHRONĀ REAKTĪVĀ DZINĒJA KONSTRUKCIJAS PĒTĪJUMI

J. Dirba, L. Lavrinoviča, R. Dobrijans

K o p s a v i l k u m s

Aplūkots sinhronais reaktīvais dzinējs ar ārējo rotoru. Analizēta dzinēja statora rievu skaita un rotora nemagnētisko barjeru ietekme uz elektromagnētisko momentu un tā pulsācijām. Parādīts, ka, palielinot rievu skaitu no $Z = 6$ uz $Z = 18$, pulsācijas koeficients samazinās aptuveni divas reizes, bet moments pieaug par 5 %. Izveidojot pētāmā sinhronā reaktīvā dzinēja ārējā rotorā papildu nemagnētiskas barjeras, momentu var palielināt par 24%.

10.01.2016.

LATVIAN JOURNAL OF PHYSICS AND TECHNICAL SCIENCES
2016, N 4

DOI: 10.1515/lpts-2016-0026

MAGNETITE NANOPARTICLES PREPARED BY SPARK EROSION

M. Maiorov[1], E. Blums[1], G. Kronkalns[1], A. Krumina[2], M. Lubane[2]

[1]Institute of Physics, University of Latvia,
32 Miera Str., Salaspils, LV2169, LATVIA
[2] Institute of Inorganic Chemistry, Riga Technical University,
32 Miera Str., Salaspils, LV2169, LATVIA
e-mail: maiorov@sal.lv

In the present research, we study a possibility of using the electric spark erosion method as an alternative to the method of chemical co-precipitation for preparation of magnetic nanoparticles. Initiation of high frequency electric discharge between coarse iron particles under a layer of distilled water allows obtaining pure magnetite nanoparticles.

Keywords*: diffraction, dynamic light scattering, magnetite, nanoparticle, superparamagnetic, X-ray.*

1. INTRODUCTION

Nanomedicine is one of the promising trends in the modern treatment methods. Due to very high specific surface of dispersed material in colloids, coating of nanoparticles with medicines allows significantly reducing their concentration in treatment, thereby eliminating the problems related to resistance of antibiotics. Magnetic nanoparticles attract special interest because they allow realizing the magnetic drug targeting or the magnetic hyperthermia. For this purpose, superparamagnetic iron oxide nanoparticles (SPIONs) are chosen [1], [2] due to their chemical inactivity. The nanoparticles as precursors are usually prepared employing various chemical methods (co-precipitation, sol-gel method, hydrothermal method, thermal decomposition). For some applications, such a technology is unacceptable because the prepared nanodispersions may contain various uncontrollable chemical side products. To obtain the magnetic nanoparticles without use of chemicals they may be prepared by initiation of high frequency electric discharge between the coarse particles of ferromagnetic metals under a layer of dielectric liquid. This results in vaporization of the metal and subsequent vapour condensation in the form of nanoparticles (Svedberg method). Such a method has been used elsewhere to prepare ferrofluids [3], [4]. In the present research, we initiate the spark erosion of iron particles that are dispersed in distilled water. In such a way, the electrically vaporized iron and water condense together as SPIONs without any side products.

2. EXPERIMENT

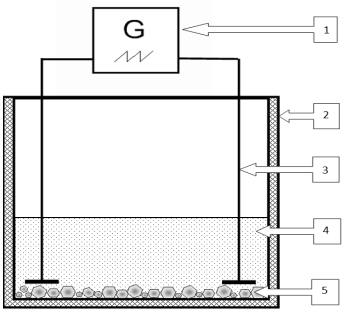

Fig. 1. Spark erosion set. 1 – spark generator, 2 – glass vessel, 3 – electrode, 4 – water, 5 –metallic particles.

The principal sketch of experimental facility is shown in Fig. 1. Thin layer of the coarse metal particles is placed on the bottom of a dielectric vessel (glass). In our experiments, we employ a pure iron powder (pharmaceutical iron Ferrum reductum) that contains particles of sizes ranging between 0.3 and 1.5 mm. The form of particles is shown in Fig. 2. The vessel is filled by distilled water. Flat steel electrodes that are in contact with the powder layer on bottom are connected to an electric spark generator. In our experiments, we used the spectrometric spark discharge generator UBI-1. Its principal circuit is shown in Fig. 3.

Adjusting the elements of discharge generator – the resistances R1 and R2, the condenser C1 and the inductor L – allows setting the mean current, the duration and the energy of discharge.

Fig. 2. Initial iron powder.

After switching on the generator, sparks appear between metal coarse particles that are suspended in a layer on bottom of the vessel. During approximately 10–20 min, the liquid in vessel gradually becomes black due to formation of nanoparticle colloidal dispersion. After that time, the colloid was separated from initial metallic coarse particles by decantation. The obtained dispersion in water is not stable, during some hours the nanoparticles precipitate on bottom of the flask. If shaking up the water suspension with hydrocarbon, in which a small amount of oleic acid is dissolved, the nanoparticles extract from water to the hydrocarbon. Oleic acid acts as a surfactant; therefore, the peptized nanodispersion is sedimentation-stable, and nanoparticles precipitation do not appear.

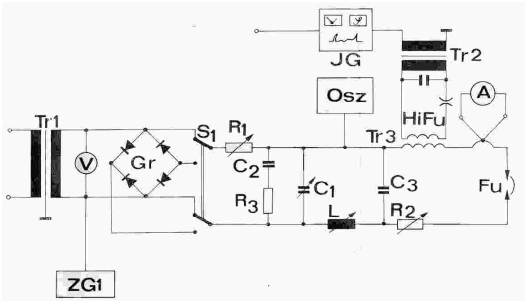

Fig. 3. Electric discharge generator UBI-1 (spark mode). A – discharge current meter, C_1 – spark capacitor, C_2 – capacitor of filter, C_3 – capacitor of high frequency loop, Fu – main discharger, Gr – AC/DC converter, HiFu – launching discharger, JG – launching generator, L – spark loop inductance, Osz – oscillograph, R_1 – current regulator, R_2 - spark loop resistor, R_3 – resistor of filter, S_1 – AC/DC switch, Tr_1 – power transformer, Tr_2 – pulse transformer, Tr_3 – transformer of launch pulse, V – voltmeter.

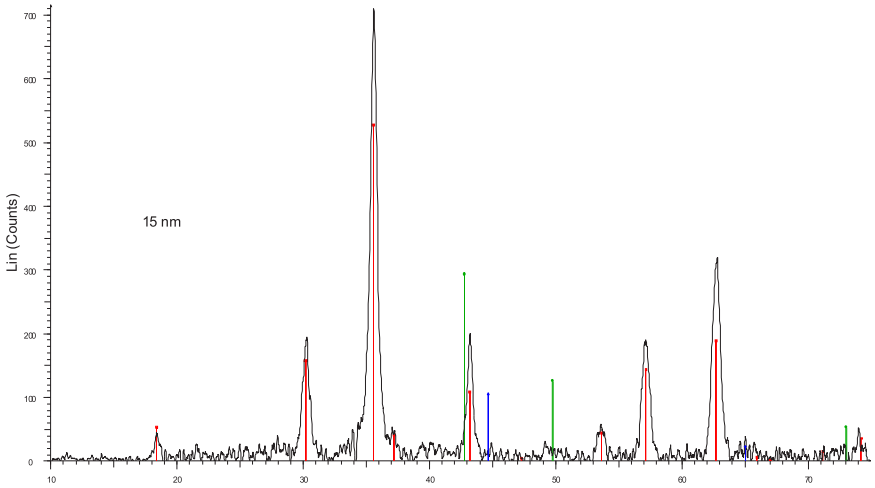

Fig. 4. X-ray diffraction of nanoparticles precipitated from water suspension.
Red lines – the magnetite peaks, green lines and blue lines – the metallic iron peaks.

The properties of the product were studied by various methods. We performed X-ray diffraction spectra measurements by the diffractometer D8 Advance (Bruker Corporation) with CuKα radiation (λ =1.5418Å). Spectral distribution of measured pikes was used to detect the chemical structure of eroded nanoparticles, whereas the form of diffraction pikes allowed evaluating the particle mean size by Scherer method. The particle size was also analysed by translation electronic microscopy data (TEM) obtained by the JEOL JEM 1230 operating at 100 kV. Additionally, the particle size distribution was analysed by employing indirect methods from the dynamic light scattering data measured by Zetasizer Nano instrument Nano S90 ZEN1690, as well as from the magnetization curves measured at room temperature by vibration sample magnetometer (Lake Shore Cryotronics, Inc., model 7404) with a maximum magnetic field of 1 T.

3. RESULTS

X-ray diffraction spectrum of nanoparticles that are precipitated from water suspension by decantation from the entire dispersion with coarse particles is shown in Fig. 4. All peaks are identified as belonging to magnetite; no metallic iron peaks are detected. It means that due to high temperatures, the electrically molten metal in sparks chemically reacts with the simultaneously vaporized water and, therefore, after solidification the nanoparticles consist of ferrous oxides, in our case – of magnetite. Form of diffraction peaks allows evaluating the particle size. According to Sheerer method, the widening of peaks corresponds to particle size of about 15 nm.

Figure 5 depicts the magnetization loop of dry powder of nanoparticles. No coercivity is observed, the magnetic saturation of powder is about 60 emu/g. It corresponds to approximately 60% bulk magnetite [5]. Nanometer sized particles have superparamagnetic properties. Summary magnetization curve of polydisperse particle suspensions may be considered superposition of Langevin functions of their various sub-fractions. The obtained oleic acid-coated nanoparticle dispersion in tet-

radecane is stable enough to allow performing the analysis of magnetization curve by decomposition it on a sum of Langevin functions of various size subfractions (the magnetogranulometry procedure [6]). The obtained particle "magnetic size" distribution is shown in Fig. 6. The volume distribution mode is 9 nm; the full distribution width at half maximum is 5.5 nm. For a comparison, Fig. 6 presents the results of particle size distribution found from the analysis of particle Brownian motion in the hydrocarbon-based suspension by Dynamic Light Scattering (DSL) measurements [7]. As it is seen, the obtained values (volume distribution mode 8.9 nm and full distribution width at half-maximum 4 nm) agree very well with the results of magnetogranulometry procedure listed above.

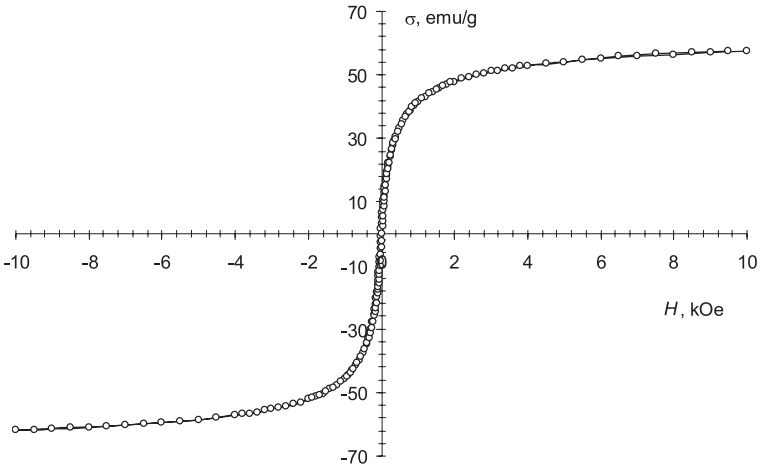

Fig. 5. The magnetization loop of the nanoparticle dry powder.

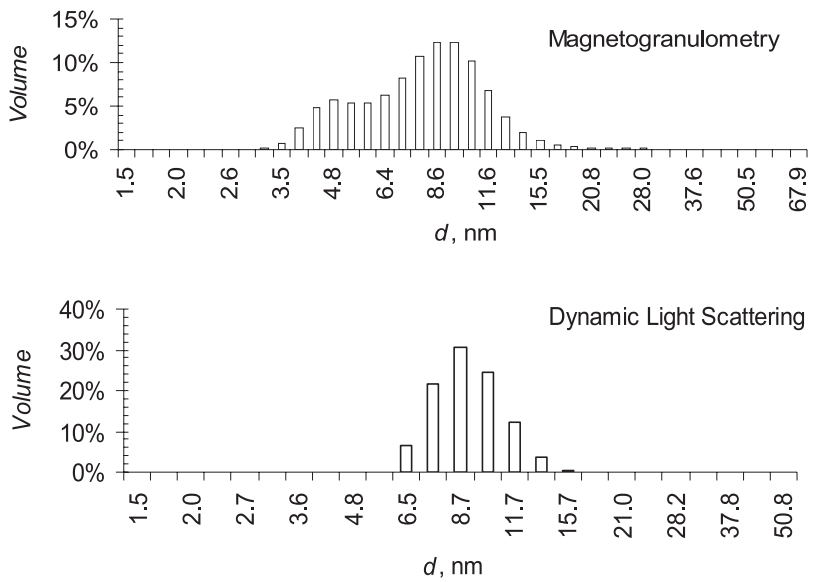

Fig. 6. The particle "magnetic" size distribution according to magnetoranulometry data (above) and the "physical" size distribution found from DLS measurements (below).

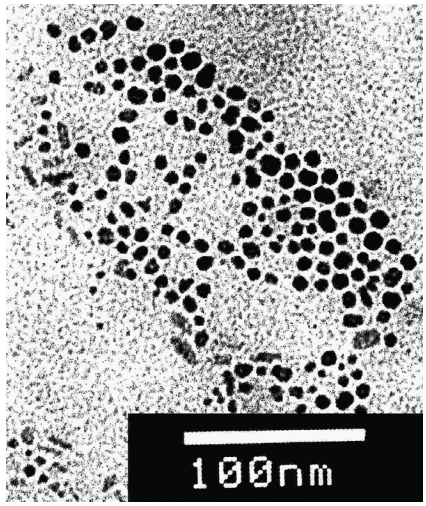

Fig. 7. TEM picture of nanoparticles dispersed in tetradecane.

Figure 7 presents the picture of nanoparticles suspended in tetradecane. As it is seen, the particle size ranges in the interval from 3 nm to 15 nm. This result also agrees relatively well with those obtained from magnetogranulometry analysis and from DSL measurements.

It would be of a special interest to obtain pure metal nanoparticles by the Swedberg method. Unfortunately, as a rule, the spark erosion in liquids is accompanied by formation of various compounds (usually carbides in alcohols and in other hydrocarbons). Our preliminary experiments say that pure iron nanoparticles may be obtained by employing argon as the dispersion media. However, the stabilization of particle dispersions in any liquid is problematic due to extremely high chemical activity of nano-sized iron.

4. CONCLUSION

The use of the Svedberg method for dispersing of metallic iron in water allows obtaining magnetic nanoparticles, which consist of magnetite due to chemical interaction of molten metal with the evaporated water in sparks during the condensation and solidification. The extraction of nanoparticles from water to hydrocarbon solvent with oleic acid as surfactant creates stable colloidal solution with superparamagnetic properties. The particle sizes that are detected by different methods (TEM, XRD, DLS and magneto granulometry) have almost identical values. The particle size distribution is sufficiently narrow.

ACKNOWLEDGEMENTS

The research has been supported by the Latvian Science Foundation, Project 286/2012 and by the Latvian State Research Programme IMIS-2.

REFERENCES

1. Tartaj, P., Morales M. P., Veintemillas-Verdaguer, S., Gonzalez-Carreno, T., and Serna, C. J. (2003). The preparation of magnetic nanoparticles for applications in biomedicine. *J. Phys. D: Appl. Phys*. *36,* R182–R197.
2. Mahmoudi, M., Sant, S., Wang, B., Laurent, S., and Sen, T. (2011). Superparamagnetic iron oxide nanoparticles (SPIONs): Development, surface modification and applications in chemotherapy. *Advanced Drug Delivery Reviews. 63*, 24–46.
3. Mozgovoi, E., N., and Blum, E. Ya. (1971). Magnetic properties of finely dispersed ferrosuspensions synthesized by the electrical condensation method, *Magnetohydrodynamics (Engl. Transl.). 7,* (4), 448–453.
4. Berkowitz, A. E., and Walter, J. L. Ferrofluids prepared by spark erosion. (1983). *Journal of Magnetism and Magnetic Materials.* 39, (1–2), 75–78.
5. Bozorth, R. (1951). *Ferromagnetism*. Toronto-New York-Landon: Van Norstand.
6. Maiorov, M. M., Blums, E., and Raj, K. (2010). Inverse task for evaluation of particle size distribution of polydisperse magnetic fluids. *(12th International Conference on Magnetic Fluids). Physics Procedia*. 9, 74–77.
7. Tech Note: Dynamic Light Scattering: An Introduction. Available at http://www.malvern.com

DZIRKSTS EROZIJAS PROCESĀ IEGŪTĀS MAGNETĪTA NANODAĻIŅAS

M. Maiorov, E.Blūms, G. Kroņkalns,
A.Krūmiņa, M. Lubāne

K o p s a v i l k u m s

Darbā tiek pētīta iespēja izmantot elektriskās dzirksts erozijas metodi kā alternatīvu ķīmiskās izsēdināšanas metodei, lai iegūtu magnētiskas nanodaļiņas. Inicējot augstas frekvences elektrisko dzirksti starp dzelzs daļiņām ūdens suspenzijā, tiek iegūtas tīra magnetīta nanodaļiņas.

17.03.2016.

LATVIAN JOURNAL OF PHYSICS AND TECHNICAL SCIENCES
2016, N 4

DOI: 10.1515/lpts-2016-0027

MAGNETIC FIELD CONTROL OF COMBUSTION DYNAMICS

I. Barmina, R. Valdmanis, M. Zake,
Institute of Physics, University of Latvia,
32 Miera Str., Salaspils, LV-2169, LATVIA,
e-mail: mzfi@sal.lv
H. Kalis, M. Marinaki, U. Strautins
Institute of Mathematics and Informatics, University of Latvia, Riga
29 Raina Blvd., Riga, LV-1459, LATVIA
e-mail: kalis@lanet.lv

Experimental studies and mathematical modelling of the effects of magnetic field on combustion dynamics at thermo-chemical conversion of biomass are carried out with the aim of providing control of the processes developing in the reaction zone of swirling flame. The joint research of the magnetic field effect on the combustion dynamics includes the estimation of this effect on the formation of the swirling flame dynamics, flame temperature and composition, providing analysis of the magnetic field effects on the flame characteristics. The results of experiments have shown that the magnetic field exerts the influence on the flow velocity components by enhancing a swirl motion in the flame reaction zone with swirl-enhanced mixing of the axial flow of volatiles with cold air swirl, by cooling the flame reaction zone and by limiting the thermo-chemical conversion of volatiles. Mathematical modelling of magnetic field effect on the formation of the flame dynamics confirms that the electromagnetic force, which is induced by the electric current surrounding the flame, leads to field-enhanced increase of flow vorticity by enhancing mixing of the reactants. The magnetic field effect on the flame temperature and rate of reactions leads to conclusion that field-enhanced increase of the flow vorticity results in flame cooling by limiting the chemical conversion of the reactants.

Keywords: *combustion of volatiles, flame composition, magnetic field forces, mixing of reactants, swirling flow dynamics*

1. INTRODUCTION

Different processes of thermo-chemical conversion of biomass, such as pyrolysis, gasification and combustion, have been developed to enhance the utilization of biomass residues (wood, straw, etc.) with large-scale variations of their composition and energy content determining variations of the heat and energy production and composition of the products. To provide stabilization of these processes, different types of combustion control can be used, such as swirl-enhanced stabilization of the

flame reaction zone [1], co-firing of a biomass with fossil fuel [2], electro-dynamic [3], [4] and magnetic field [5], [6] control of combustion dynamics. The previous experimental study of the magnetic field effects on the flame formation and combustion characteristics has shown that application of the magnetic field to the flame can result in significant changes in flame shape, size and combustion characteristics due to development of the processes, which can be related to gradient magnetic field-induced mass transport of paramagnetic flame species [6]. In addition to gradient magnetic field effect on the mass transport of paramagnetic flame species development of combustion dynamics downstream, the combustor can be affected by the magnetic field-induced force, which acts on the movement of charged flame species. Thus, the main aim of the recent study is to provide a complex mathematical modelling and experimental study of the magnetic field-induced variations of the combustion dynamics with estimation of the effect, which can be related to the effect of the magnetic force on the movement of charged flame species (positive ions).

Mathematical model is developed with account of the axial and azimuthal components of flow velocity and development of the exothermic reaction of fuel combustion downstream the cylindrical combustor with radius r_0. The flame flow formation with axial velocity at the inlet of the combustor (U_0) is affected by the radial (B_r) and axial (B_z) components of the axially symmetric magnetic field B_0. The magnetic field is induced by direct electric current of a density j_0 in a coil, which is placed at the inlet of the combustor, close to the inner surface of the combustor by surrounding the flame flow. The distribution of a stream function, azimuthal component of velocity (V_0), vorticity and the formation of the velocity and temperature profiles are calculated by varying the electrodynamic force parameter $P_e = \frac{B_0 j_0 r_0}{\rho_0 U_0^2}$ and swirl number $S = \frac{V_0}{U_o}$. The results of numerical simulation have shown that an increase of the electrodynamic force parameter P_e results in a magnetic field-enhanced increase of the maximal flow velocity raising flow vorticity, whilst decreasing peak flame temperature and the rate of reaction.

2. MATHEMATICAL MODELLING

The present investigation continues the study of Choi, Rusak et al. [7] and Kalis et al. [8] by conducting a numerical investigation of the axially symmetric, steady swirling flow in a cylindrical pipe using the low Mach number approximation. The swirling flow with axial (u_z), radial (u_r), and azimuthal (u_φ) components of velocity is developing downstream the pipe. The axial velocity determines the formation of a uniform stream in a central part of the cylindrical pipe-inlet. The azimuthal velocity with rotation of the part from tube inlet is obtained. Similar experiment with turbulent is considered in [9].

The approximate mathematical model takes into account the development of time-dependent exothermic reaction downstream the cylindrical pipe of radius r' = r_0 = 0.05 [m] and of a length z = z_0 = 0.1 [m]. The temperature dependence of the reaction rate is estimated using first-order Arrhenius kinetics. At the pipe inlet: T_0 = 300 K, mass fraction of combustible reactant C_0 =1 mol/m^3 and flow density ρ_0 = 1 kg/m^3.

The aim of mathematical modelling is to understand how a flow structure is affected by a direct electric current of density j_0 [A/m^2] in the annular wire coil, which is positioned at the pipe inlet (z = 0) close to the internal wall of the pipe (combustor) and surrounds the flame flow. At the pipe inlet, the uniform flow field formation with the axial flow velocity U = U$_0$ = 0.01 [m/s] in the central part of a pipe $r' \le r_1' = r_0 / 2$ is considered.

The following dimensionless values

$r = (r_0)^{-1} r' \in [0,1]$, $x = (r_0)^{-1} z \in [0, x_0]$, $\left(x_0 = (r_0)^{-1} z_0 = 2\right)$,

$t = (r_0 / U_0)^{-1} t' > 0$, $w = (U_0)^{-1} u_z$, $v = (V_0)^{-1} u_\theta$, $u = (U_0)^{-1} u_r$,

$T = (T_0)^{-1} T'$, $\rho = (\rho_0)^{-1} \rho'$ are used for numerical simulation. V_0 is the maximal value of the azimuthal velocity.

The flow boundary (r = 1) is subjected to a heat loss due to Newtonian cooling at temperature T_0 of surroundings and heat transfer coefficient h = 0.1 [J/sm^{2}K].

The current in a coil induces the radial B_r and axial B_z components of the induced magnetic field B in the ionized gas flow, which leads to the formation of the axial $F_z = -B_r j_0$ and radial $F_r = B_z j_0$ components of the electromagnetic force (Lorentz' force) F and the azimuthal component of the curl of the force $f_\phi = rot_\phi F = \partial F_r / \partial z - \partial F_z / \partial r'$. From $div(B) = \partial B_r / \partial r' + \partial B_z / \partial z + B_r / r' = 0$ it follows that $f_\phi = -j_0 B_r / r'$.

The distribution of electromagnetic fields for the axially-symmetric system of electric current has been investigated and calculated similarly using the azimuthal component A$_\varphi$ of the vector potential and the Biot-Savart law [10].

With this approximation:

$$B_r = \frac{\mu I}{2\pi} \frac{z}{cr'} \left(\frac{z^2 + r_0^2 + r'^2}{z^2 + (r_0 - r')^2} E(k) - K(k) \right),$$

$$B_z = \frac{\mu I}{2\pi c} \left(-\frac{z^2 + r_0^2 + r'^2}{z^2 + (r_0 - r')^2} E(k) + K(k) \right),$$

$$A_\varphi = \frac{\mu I}{2\pi} \frac{1}{c} \left(\frac{2 - k^2}{2} K(k) - E(k) \right), \text{ where } k = 2\sqrt{r_0 r'} / c,$$

$c = \sqrt{(r_0 + r')^2 + z^2}$, $K(k)$, $E(k)$ are the total elliptical integral of first and second kind, B$_s$ = -r' A$_\varphi$ is the magnetic stream function, $B_r = \partial A_\varphi / \partial z, B_z = \partial A_\varphi / \partial r + A_\varphi / r'.$

For numerical solutions we eliminate the modified pressure p* from the hydrodynamic equations by introducing the stream function ψ with the following expressions:

$r\rho w = \partial\psi / \partial r, r\rho u = \partial\ \psi / \partial x\ (\rho = 1/T)$, $p^* = p - j_0 A_\varphi$, $f_\phi = -j_0 B_r / r'$.

For deleting the source terms $u v / r,\ u \zeta / r$ in the equations, the transformation is used for the circulation $\tilde{v} = v r$ and for modified vorticity $\tilde{\zeta} = \zeta / r$. Then equations for vorticity and stream function are given by:

$$\begin{cases} \dfrac{\partial\tilde{\zeta}}{\partial t} + u\dfrac{\partial\tilde{\zeta}}{\partial r} + w\dfrac{\partial\tilde{\zeta}}{\partial x} + 0.5\dfrac{T}{r}J\left(T^{-1}, V^2\right) = \dfrac{S^2 T}{r^4}\dfrac{\partial(T^{-1}\tilde{v}^2)}{\partial x} - P_e\dfrac{\tilde{B}_r}{r^2}, \\ \dfrac{\partial\psi}{\partial t} = \dfrac{\partial}{\partial x}\left(T\dfrac{\partial\psi}{\partial x}\right) + r\dfrac{\partial}{\partial r}\left(\dfrac{T}{r}\dfrac{\partial\psi}{\partial r}\right) + r^2\tilde{\zeta}, \dfrac{\partial\tilde{v}}{\partial t} + u\dfrac{\partial\tilde{v}}{\partial r} + w\dfrac{\partial\tilde{v}}{\partial x} = 0, \end{cases} \tag{1}$$

where the second equation for numerical simulation is transformed to non-steady, $V = \sqrt{u^2 + w^2}$ is the module of velocity, $\tilde{B}_r = \dfrac{B_r}{B_0}$, $B_0 = \dfrac{\mu I}{2\pi r_0} = 0.410^{-5} I[T]$, $J(a,b) = \dfrac{\partial a}{\partial x}\dfrac{\partial b}{\partial r} - \dfrac{\partial a}{\partial r}\dfrac{\partial b}{\partial x}$ is the Jacobian, $\zeta = \dfrac{\partial u}{\partial x} - \dfrac{\partial w}{\partial r}$, $P_e = \dfrac{B_0 j_0 r_0}{\rho_0 U_0^2}$ is the electrodynamical force parameter, $S = \dfrac{V_0}{U_0}$ is the swirl number.

2-D reaction-diffusion equation system of two nonlinear partial differential equations is used to estimate the formation of the flow temperature and composition fields:

$$\begin{cases} \dfrac{\partial T}{\partial t} + u\dfrac{\partial T}{\partial r} + w\dfrac{\partial T}{\partial x} = \dfrac{L_e}{\rho Pe}\Delta T + \beta AC\exp\left(-\dfrac{\delta}{T}\right), \\ \dfrac{\partial C}{\partial t} + u\dfrac{\partial C}{\partial r} + w\dfrac{\partial C}{\partial x} = \dfrac{1}{\rho Pe}\Delta C - AC\exp\left(-\dfrac{\delta}{T}\right), \end{cases} \tag{2}$$

where $\rho\ T = 1$. $Pe = \dfrac{\rho_0 U_0 r_0}{D} = 10$, $L_e = \dfrac{\lambda}{c_p D} = 1$ are Peclet and Lewis numbers, $\beta = \dfrac{B}{c_p T_0} = 5$ is the heat-release parameter, $\delta = \dfrac{E}{R T_0} = 10$ – the scaled activation-energy, Δ is the Laplace operator, $D = 5.e-5[m^2/s]$ is the molecular diffusivity, $\lambda = 5.e-2[J/s\,m\,K]$ – the thermal conductivity, $c_p = 1000[J/kg\,K]$ – the specific heat at constant pressure, $B = 1.5e+6[J/kg]$, $A = \dfrac{A' r_0}{U_0}\left(A' = 1.e+4[1/s]\right)$, $E = 2.5e+4[J/mol]$ are the specific heat release, the pre-exponential factor of reaction rate and the activation energy, $R = 8.314[J/mol\,K]$ – the universal gas constant.

The boundary conditions are the following:

1) along the axis r = 0 - $\widetilde{v}=0$, $\psi=0$, $\partial T/\partial r=\partial C/\partial r=\partial\widetilde{\zeta}/\partial r=0$ (the symmetry conditions),

2) at the wall r = 1 - $\widetilde{v}=0$, $\psi=q$, $\widetilde{\zeta}=0$, $\partial T/\partial r=\partial C/\partial r=0$,

3) at the pipe outlet x = x_0 -

$u=0$, $\partial T/\partial x=\partial C/\partial x=\partial\widetilde{\zeta}/\partial x=\partial\widetilde{v}/\partial x=\partial\psi/\partial x=0$,

4) at the pipe inlet x=0 - $u=0, \widetilde{\zeta}=0$ $T=1$, for $r\in[0,1]$ and $w=1$, $C=1$, $\psi=0.5r^2$, $\widetilde{v}=0$, for $r\in[0,r_1]$; $\psi=q$, $\widetilde{v}=4r\dfrac{(r-r_1)(1-r)}{(1-r_1)^2}$, $w=0$, $C=0$ -

we have uniform jet flow by $r<r_1$ and rotation by $r>r_1$ with maximal azimuthal velocity 1 by $r=(1-r_1)/2$.

Here $Bi=\dfrac{hr_0}{\lambda}$ is the Biot number, $q=\dfrac{r_1^2}{2}$ is the dimensionless fluid volume. The dimensionless radial and axial distribution of the magnetic field induction and magnetic field stream (B_r, B_z and B_s) for $B_0=1$ is represented in Fig. 1, a-c.

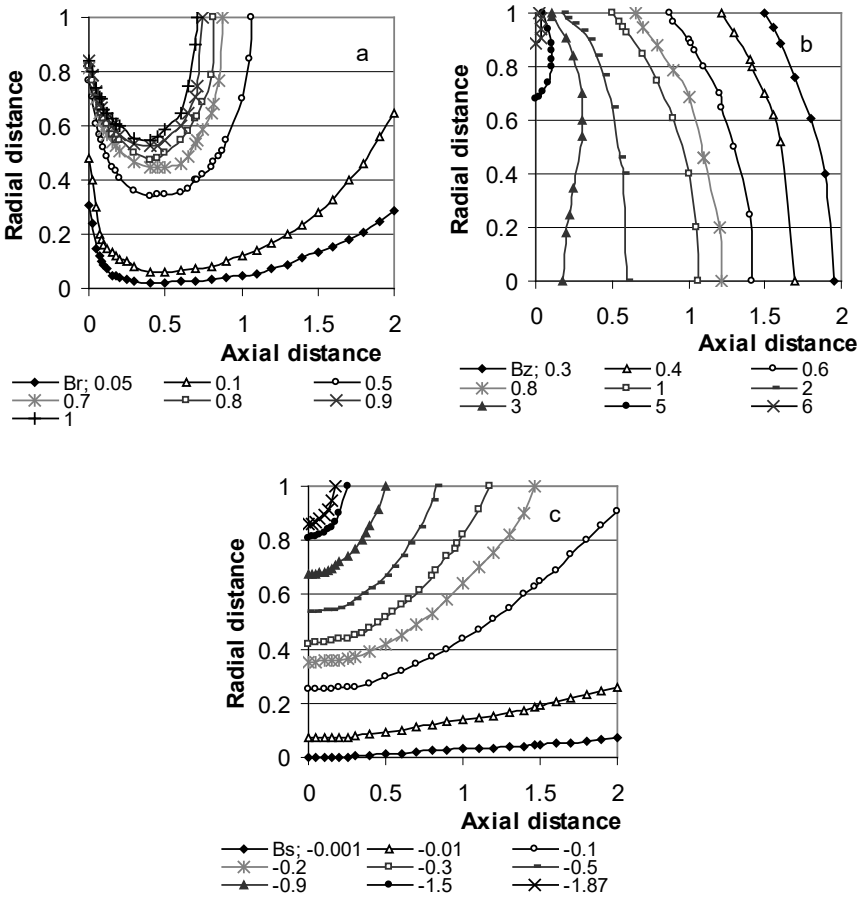

Fig. 1. The dimensionless distribution of the axial and radial components (a, b) of the magnetic field induction and magnetic field stream function (c).

The approach seeks the steady solution as the time asymptotic limit of the solutions of the unsteady equations. The distribution of stream function, azimuthal component of velocity, vorticity (Fig. 2) and temperature (Fig. 3) has been calculated using the implicit FDS with the upwind differences in the space, ADI method and under-relaxation.

For numerical simulation, the following parameters are used: S = 1;3, $r_1 = 0.5$, A = 50000, *Bi* – 0.1, P_e = 0;0.1;0.5;1, $\tau = 0.0008$, *It* = 2500 (number of iterations or time steps).

The results of numerical simulation are given in Table 1, where T_{av} is the averaged value of the flow temperature and $\widetilde{R} = AC\exp(-\delta / T)$ is the reaction rate.

Table 1

The values of $P_e, S, T_{av}, \max U, \max \widetilde{R}, \max T, \max|\zeta|, \min\psi$ **for** $x_0 = 2$

P_e	S	T_{av}	$\max U$	$\max R$	$\max T$	$\max\|\zeta\|$	$\min\psi$
0.0	1	3.000	5.402	805.97	5.877	137.61	0
0.5	1	2.883	5.463	805.29	5.873	139.85	-0.0056
1.0	1	2.759	5.545	804.97	5.861	143.38	-0.0460
0.0	3	2.994	5.409	805.94	5.877	137.96	0
0.1	3	2.975	5.422	805.86	5.876	138.05	0
0.5	3	2.880	5.477	805.24	5.873	140.00	-0.0061
1.0	3	2.733	5.579	805.07	5.862	145.20	-0.0524

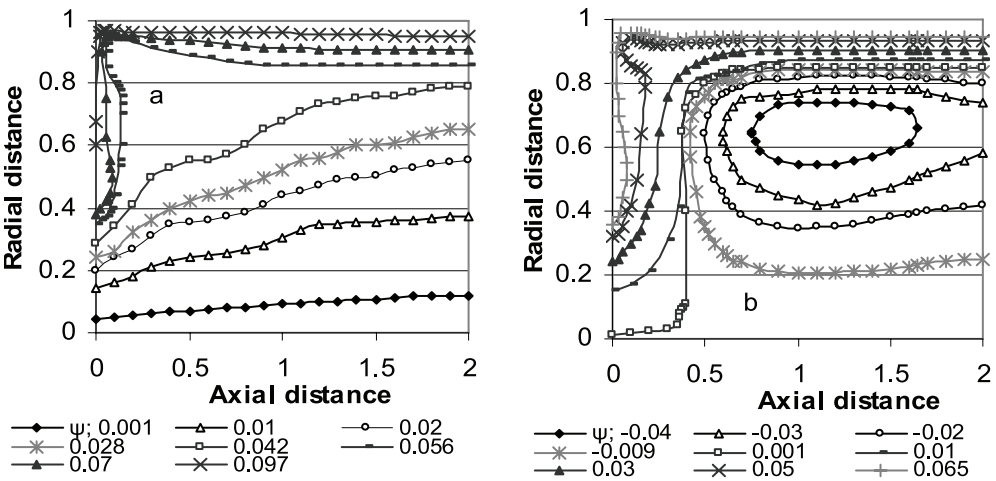

Fig. 2. Magnetic field effect on the swirling flow stream function:
a) P_e = 0; S = 1; b) P_e = 1; S = 1.

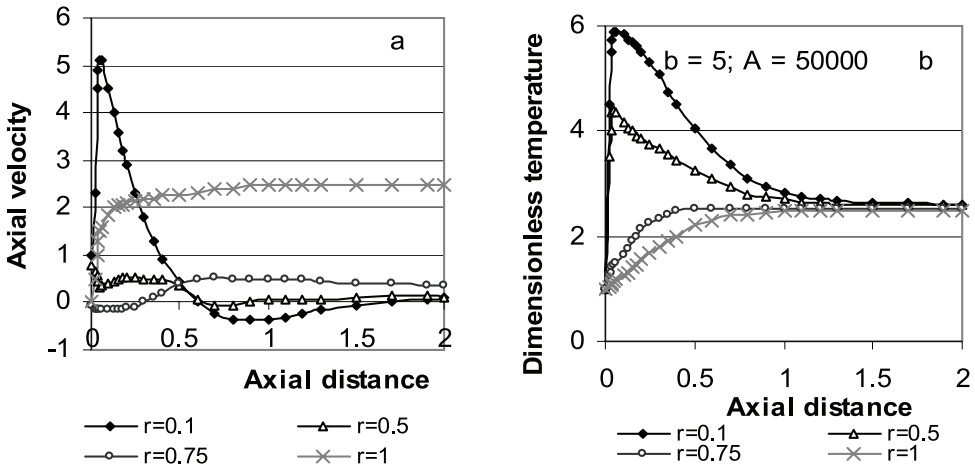

Fig. 3. The formation of dimensionless profiles of the axial velocity (a) and temperature (b) for swirling flame flow; Pe = 0.5; S = 3.

3. EXPERIMENTAL PART

Experimental study of the magnetic field effect on the combustion characteristics at thermo-chemical conversion of wood pellets was carried out using a batch-size device with integrated biomass gasifier and water cooled combustor (Fig. 4). Axially-symmetric magnetic field is applied to the flame using two coils, which are fed with a direct current. Magnetic field with induction up to 50mT acts on the flame volume from the bottom of the combustor up to a distance L/D ≈ 2 from the centre of coils. The propane flame flow (2) is used to supply additional heat energy into the upper part of biomass pellets at an average rate of 1 kJ/s to initiate the biomass gasification and the formation of the axial flow of volatiles at the inlet of the combustor. The primary air is supplied below the layer of biomass pellets at an average rate of 30–40 l/min to support a thermal decomposition of main biomass components (3). Secondary swirling air is supplied (4) above the layer of biomass at an average rate of 65 l/min and is used to provide the swirl-enhanced combustion of the volatiles developing downstream the water-cooled combustor (6).

To estimate the magnetic field effect on the combustion dynamics at thermo-chemical conversion of biomass, the local measurements of the flame velocity, temperature and composition are carried using a Pitot tube and a gas analyzer Testo-350 XL. The local measurements of the flame composition, temperature and velocity were carried out at distance z/D = 2.8 above the secondary air inlet nozzle close to the coils of electromagnet (z/D ≈ 0.2). In addition, the local online measurements of the flame temperature using Pt/Pt/Rh thermocouples were carried out at the end stage of the combustion of volatiles – at distance x/D = 6.6 above the secondary air inlet nozzle. Produced heat energy was estimated from calorimetric measurements of cooling water flow of the combustor using the PC-20 control unit.

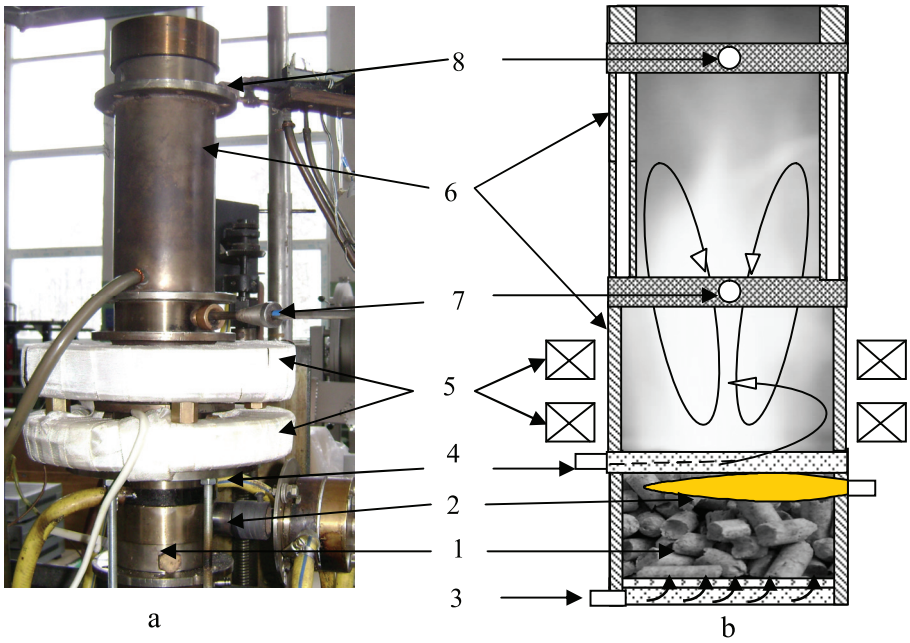

Fig. 4. A photo (a) and sketch (b) of the experimental device: biomass gasifier (1), propane flame nozzle (2), primary air supply nozzle (3), secondary air swirl nozzle (4), coils of electromagnet (5), water-cooled combustor (6), diagnostic sections (7, 8).

4. RESULTS AND DISCUSSION

4.1. Experimental Results

The formation of the flow velocity field downstream the combustor for given configuration of a pilot device is influenced by the two main factors – the axial flow of volatiles (CO, H_2, CH_4), which is determined by the thermal decomposition of biomass pellets and is supported by primary air supply, and combustion of volatiles, which is supported by secondary azimuthal air supply at the bottom of the conductor. The resulting flow field of the undisturbed flame flow (B = 0) above the coils (L = 20 mm) indicates the formation of the relatively uniform axial velocity profile across the flow centerline ($r/R < 0.7$) with average value of the axial flow velocity 1.3 m/s and large gradients of the axial and azimuthal flow velocity components and swirl intensity in the near vicinity of the channel walls ($r/R > 0.7$).

The application of the magnetic field to the flame disturbs the flow velocity profiles determining the field-induced variations of the local and average values of the axial (u_z), azimuthal (u_φ) flow velocity and swirl intensity) above the coils (Fig. 5, a, b).

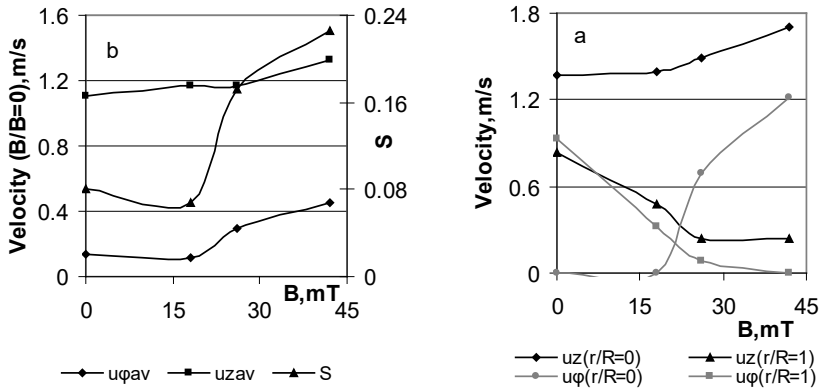

Fig. 5. The magnetic field effect on the local (a) and average values of the axial and tangential flow velocity and flow swirl number (b).

Along the outside part of the flame reaction zone (r/R > 0.7) the magnetic field-induced force slows down the axial and tangential flow velocity (Fig. 5-a) by enhancing the axial and swirl motion in the flame centerline (r/R < 0.7) with correlating increase of the average values of the axial, azimuthal flow velocities and swirl intensity (Fig. 5 b). The results of mathematical modelling have shown a similar increase of the flow vorticity by increasing the magnetic field-induced Lorentz force and magnetic force parameter P_e (Table 1). This allows suggesting that the magnetic field-induced variation of the average values of the flow velocity components and swirl intensity can be related to the effect of Lorentz force. As follows from Fig. 5, more pronounced magnetic field-induced variations indicate the azimuthal flow velocity component u_φ, for which the instant velocity vector of charged flame species $\boldsymbol{u}_\varphi$ is oriented perpendicularly to the magnetic field $\boldsymbol{B}$ determining the formation of the magnetic force $\boldsymbol{F}_m = q_i \boldsymbol{u}_\varphi \times \boldsymbol{B}$.

Moreover, from the results of numerical modelling (Table 1) it follows that the field-induced variations of the average values of the flow velocity and vorticity correlate with a field-enhanced decrease of the average and peak flame temperatures. Similar decrease of the local and average values of the flame temperature above the coils follows from the results of the experimental study indicating the field-enhanced correlating decrease of the volume fraction of CO_2, combustion efficiency and produced heat energy by increasing the magnetic field induction (Fig. 6, a-d).

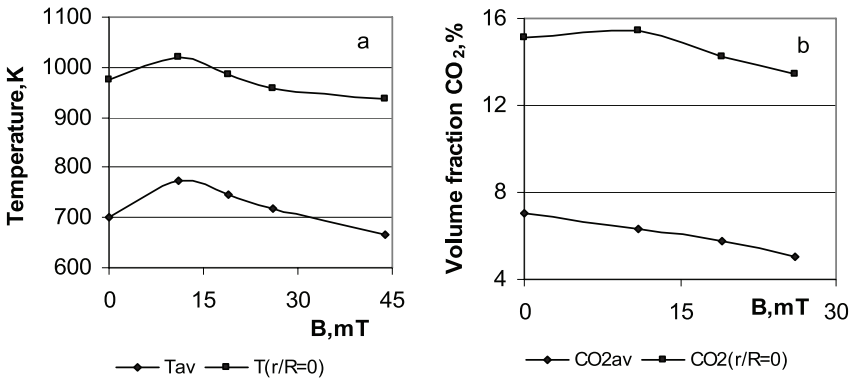

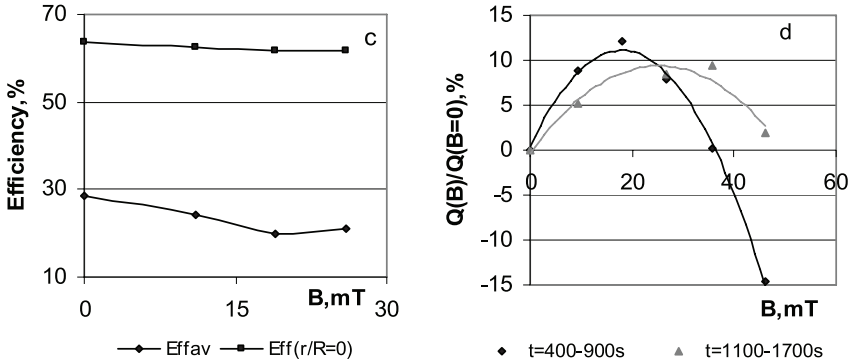

Fig. 6. The magnetic field effect on the main combustion characteristics above the coils.

Moreover, in accordance with the results of mathematical modelling, the measurements of the flame composition profiles confirm the field-induced decrease of the reaction rates by increasing the external magnetic force, which results in an increase of the mass fraction of unburned volatiles (CO, H_2) at the interface between the axial fuel flow and air swirl with field-enhanced increase of the local and average values of the air excess and correlating decrease of combustion efficiency along the outer part of the flame reaction zone. This correlation confirms the field-enhanced mixing of the axial flow of volatiles with cold air flow with resulting cooling of the flame reaction zone, which shows the direct influence on combustion dynamics by increasing the mass fraction of unburned volatiles and air excess at the interface between the axial flow of volatiles and air swirl decreasing combustion efficiency above the coils. It should be noticed that magnetic field improved mixing of the flame components along the interface is confirmed by the results of the experimental study of magnetic field effect on diffusion flames, which confirm the field-induced forcing of the oxidant stream into fuel stream [11]. By considering the impact of magnetic field effect on the mixing of the reactants, which results in cooling of the flame reaction zone, it is concluded that to restrict the field-induced decrease of the flame temperature, there is a need to provide the additional heat energy supply into the secondary swirling air flow as it follows from the results of experimental study of the magnetic field effects on the flame formation by co-firing the biomass pellets with gas (propane) [6].

4. CONCLUSIONS

The present research incorporates the mathematical modelling and experimental study of swirling flame behavior in the presence of magnetic field. Based upon the results of mathematical modelling and experimental study, the following conclusions have been drawn.

The results of mathematical modelling have shown that the magnetic field exerts the influence on the flow dynamics and the formation of the flow stream function indicating an increase of the flow vorticity and the local and average values of the flow velocity. An increase of the flow vorticity results in an enhanced mixing of

the reactants by cooling the flame reaction zone and decreasing the rate of reactions.

The results of mathematical modelling are confirmed by the experimental study of the magnetic field effects on the swirling flow dynamics and the formation of the reaction zone with estimation of the effects, which can be related to the effect of magnetic force on the azimuthal movement of charged flame species, indicating the magnetic field-enhanced swirl motion along the centerline of the flame reaction zone ($r/R < 0.7$) with dominant field effect on swirl-enhanced mixing of the axial flow of volatiles with cold air swirl.

The field-enhanced mixing of the axial flow of volatiles with cold air flow results in cooling of the flame reaction zone. The flame cooling slows down the rate of reactions with local variation of the combustion characteristics – an increase of the mass fraction of unburned volatiles, decrease of the combustion efficiency and produced heat energy.

ACKNOWLEDGEMENTS

The authors deeply acknowledge the financial support of the Latvian research grant No.623/14 and of the University of Latvia grant No. 6012-A55.2/48.

REFERENCES

1. Gupta, A.K., Lilley, D.G., & Syred, N. (1984). Swirl flows. *Abacus Press UK*, 588.
2. Sami, M., Annamalai, K., Woldridge, M. (2001). Cofiring of coal and biomass fuel blends. *Prog. Energy Combustion Sci. 27*, 171–214.
3. Lawton, J., Weinberg, F.J. (1969). Electric aspects of combustion. *Clarenton Press*, 336–340.
4. Colannino, J. (2012). Electrodynamic combustion control, TM technology. A Clear Sign White Paper, *ClearSign Combustion Corporation*, Seattle. Available at www.clearsign-combustion.com
5. Swaminathan, S. (2005). Effects of magnetic field on micro flames. *A Thesis of Master of Science in Mechanical Engineering at the Department of Mechanical Engineering*, 125. Available at http://etd.lsu.edu/docs/available/etd-11182005-092209/unrestricted/Swaminathan_thesis.pdf
6. Barmina, I., Lickrastina, A., Suzdalenko, V., & Zake, M. (2012). Gradient magnetic field promotion of pelletized biomass combustion. *Magnetohydrodynamics 48*, 351– 360.
7. Choi, J.J., Rusak, Z., & Kapila, A.K. (2007). Numerical simulation of premixed chemical reactions with swirl. *Combustion Theory and Modelling 6* (11), 863–887.
8. Kalis, H., Marinaki, M., Strautins, U., & Lietuvietis O. (2015). On the numerical simulation of the combustion process with simple chemical reaction. *Proc. of the 7th Baltic Heat Transfer conf. "Advances in Heat Transfer"*, 24–26 Aug. 2015, (pp. 175–180).
9. Buikis, A., & Kalis, H. (2004). Flow and temperature calculation of electrolyte for a finite cylinder in the alternating field of finite number circular wires. *Magnetohydrodynamics 40* (1), 77–90.
10. Buikis, A., & Kalis, H. (2004). Creation of temperature field in a finite cylinder by alternated electromagnetic force. *Progress in Industrial Mathematics at ECMI 2002*, 247–251.

11. Thompson, J.I. (1994). Computational modeling of Lorentz force induced mixing in alkali seeded diffusion flames. *A thesis for the degree of Master of Science*. Oregon State University. Available at
12. https://ir.library.oregonstate.edu/xmlui/bitstream/handle/1957/35563/ThompsonJonIra1995.pdf?sequence=1

MAGNĒTISKĀ LAUKA IETEKME UZ DEGŠANAS PROCESU DINAMIKU

I. Barmina, R. Valdmanis, M. Zaķe,
H. Kalis M. Marinaki, U. Strautiņš

K o p s a v i l k u m s

Ir veikti kompleksi pētījumi par magnētiskā lauka ietekmi uz liesmas virpuļplūsmu dinamiku, kas apvieno plūsmas matemātisko modelēšanu un eksperimentālos pētījumus, izvērtējot galvenos faktorus, kas ietekmē šo plūsmu dinamikas veidošanos magnētisko spēku laukā.

Plūsmas dinamikas matemātiskā modelēšana apliecina, ka magnētiskais lauks izraisa plūsmas struktūras izmaiņas, intensificējot lokālu virpuļu veidošanos reakcijas zonā, kas izraisa plūsmas vidējā ātruma palielināšanos ar vienlaicīgu reakcijas zonas vidējās un maksimālas temperatūras samazināšanos, kas līdz ar to samazinot ķīmisko reakciju ātrumu degšanas zonā.

Līdzīgs rezultāts ir iegūts, arī veicot eksperimentālos pētījumus par magnētiskā lauka ietekmi uz virpuļplūsmas dinamiku, sastāvu un temperatūru, kas apliecina, ka plūsmas azimutālā ātruma izmaiņas magnētiskā laukā sekmē gaistošo savienojumu aksiālās plūsmas sajaukšanos ar gaisa virpuļplūsmu, izraisot degšanas zonas temperatūras, degšanas procesu efektivitātes un saražotā siltuma daudzuma samazināšanos, ierobežojot gaistošo savienojumu degšanas zonas veidošanos.

01.06.2016.

LATVIAN JOURNAL OF PHYSICS AND TECHNICAL SCIENCES
2016, N 4

DOI: 10.1515/lpts-2016-0028

LIMITS TO CO_2-NEUTRALITY OF BURNING WOOD. (REVIEW)

J. Abolins[1,2]*, J. Gravitis[2]

[1] Institute of Atomic Physics and Spectroscopy, University of Latvia,
19 Raina Blvd., Riga, LV-1586, LATVIA
[2] Latvian State Institute of Wood Chemistry,
27 Dzerbenes Str., Riga, LV-1006, LATVIA
*e-mail: jclover@latnet.lv

Consumption of wood as a source of energy is discussed with respect to efficiency and restraints to ensure sustainability of the environment on the grounds of a simple analytical model describing dynamics of biomass accumulation in forest stands – a particular case of the well-known empirical Richards' equation. Amounts of wood harvested under conditions of maximum productivity of forest land are presented in units normalised with respect to the maximum of the mean annual increment and used to determine the limits of CO_2-neutrality. The ecological "footprint" defined by the area of growing stands necessary to absorb the excess amount of CO_2 annually released from burning biomass is shown to be equal to the land area of a plantation providing sustainable supply of fire-wood.

Keywords: *bioenergy, limits to CO_2-neutrality, sustainable supply, wood.*

1. INTRODUCTION

Sustainable consumption of renewable resources is limited by the rate of regeneration. Land area and radiation available on the area are two core factors determining regeneration of any kind of biomass while the rate depends on the productivity of the biological species – the rate of amassing wood by photosynthesis. Perennials have the advantage of accelerating the growth with time while keeping the accumulated biomass stored.

The use of biomass as a renewable source of energy has additional constraints imposed by sustainability with regard to environment the main concern being release of greenhouse gases affecting stability of the global climate. Despite the corporate belief of biofuels being neutral to CO_2 emissions [1]–[3], the subject is contentious [4]–[7] although authors of more scrupulous recent studies recognise delayed sequestration of carbon released by using biomass for energy [8]–[10] and point to radical disparity between the amounts of carbon released and recaptured [11]. The subject still requires a proper discussion and relevant argumentation provid-

ing grounds for understanding dynamics of the basic carbon cycle from biomass to atmosphere and back to biomass. The study presented to the attention of the reader considers the boundaries and factors imposed by CO_2-neutrality of wood as a source of primary energy.

2. BASIC DEFINITIONS AND THE METHOD

Since usage of wood fuel for electricity generation is extremely wasteful use of bioenergy and land assets [12], 16] and, therefore, unsustainable, hereafter attention is paid to burning wood for purposes of heating having a distinctly seasonal character at higher altitudes. Energy is consumed at the time of year when photosynthesis fixing carbon dioxide into new biomass is not active for which reason the gas released at burning wood accumulates in the atmosphere the current process being not CO_2-neutral. Therefore, it is reasonable to define the CO_2-neutrality with respect to the whole seasonal cycle: burning wood is CO_2-neutral if the annual amount of carbon dioxide released into the atmosphere is balanced by the annual amount of carbon dioxide sequestered from the atmosphere by photosynthesis and stored again in biomass. The definition implies that burning biomass is sustainable with respect to the resource and climate if the annual amount of biomass burnt is equal to the annual amount of biomass grown.

The **C**urrent **A**nnual **I**ncrement of wood biomass of a natural even-aged forest stand defined as the amount of stock accumulated during the year at the particular age is presented as the derivative of stock *S* with respect to time *t* representing the rate of growth *R* as function of time at the particular instant:

$$R(t) = \frac{dS(t)}{dt}. \tag{1}$$

The Mean Annual Increment defined by the ratio of the stock S(t) at a particular age t to the age represents the productivity P(t) of the stand at that age as function of time:

$$P(t) = \frac{S(t)}{t}. \tag{2}$$

The rate of growth expressed by (2) and stock are obviously interrelated by

$$S(t) = \int dtR(t). \tag{3}$$

It should be noted that the current annual increment being of a finite magnitude here is presented by (2) – the rate of growth as a continuous function defined for any infinitesimal instant of time. Nevertheless, the apparent inconsistency is resolved by interpreting the rate of growth as the annual increment at the respective instance of time – the annual acquisition of biomass being projected to the instant value of the rate of growth. The finite amount of stock accumulated by the stand within a particular year-long time interval $\Delta t = t_n - t_{n-1}$ under these assumptions is expressed by

$$\Delta S_n = \int_{t_{n-1}}^{t_n} dt \cdot R(t). \tag{4}$$

Dynamics of biomass accumulation in a forest stand [13] derived from the rate of growth assumed being proportional to the active light-absorbing area of the canopy is presented by Richards' equation [14]:

$$S(t) = (1 - e^{-bt})^c \tag{5}$$

with parameter values $b = ln2$ and $c = 2$ found for dimensionless time scale $x = \frac{t}{t_m}$ normalised with respect to the time t_m at which the function derived for the rate of growth

$$R(t) = const \cdot \left(1 - e^{-bt}\right) \cdot e^{-bt} \tag{6}$$

reaches the maximum. The rate of growth normalised to its maximum value at $x = 1$ as function of the normalised time variable x is presented by equation

$$R(x) = 4 \cdot \left(1 - e^{-xln2}\right) \cdot e^{-xln2} \tag{7}$$

and the stock normalised to its maximum limit S_∞ at $x = \infty$ – by equation

$$\frac{S(x)}{S_\infty} = \left(1 - e^{-xln2}\right)^2 \tag{8}$$

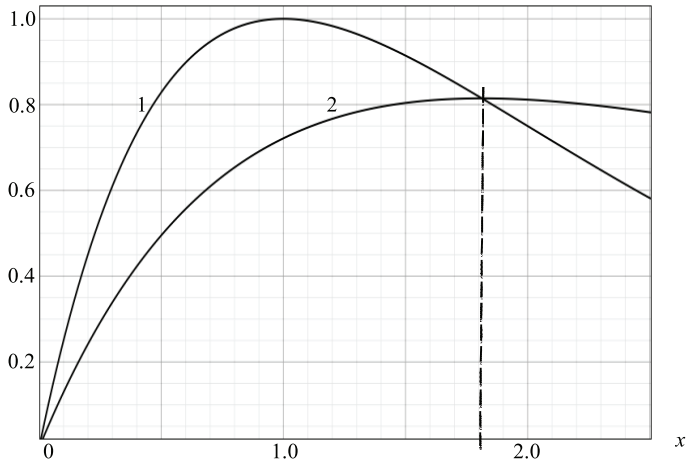

Fig. 1. Rate of growth (1) and productivity (2) – the mean annual increment in normalised coordinates.

Graphs of the rate of growth (7) and productivity P(x) are presented in Fig. 1. The scale of the ordinate axis is normalised to the maximum of the current annual increment relative to which the maximum value of the mean annual increment is about 0.8 and is reached at the normalised age of $x \approx 1.81$ – the age of maximum productivity of the stand area and the optimum cutting age providing the highest land-use efficiency. The stock (yield) of wood biomass at this age calculated from (8) is about 0.50812, which is slightly more than twice the stock ($S = 0.25$) at the age of maximum rate of growth (at $x = 1$).

Accumulation of biomass represented by (7) and (8) is defined by a single parameter – the age t_m, at which the rate of growth of a particular stand reaches its maximum. This single parameter, apart from the bio-potential of the species, implies and presents an integrated result of the site characteristics – such as fertility, period of vegetation, availability of water and light, etc. affecting the rate of biomass accumulation.

The current annual uptake of biomass and, consequently, the atmospheric carbon is calculated from (8) as the difference of stock between the year number $n + 1$ and n the increment ΔS being evaluated in units of stock S_o at the age of land productivity optimum at $x_o \approx 1.81$

$$\Delta S_n = \frac{S_n - S_{n-1}}{S_o},\ n = 1, 2, \ldots n_c;\ S_o = S(x_o) \neq S_0 = 0. \quad (9)$$

For that purpose the normalised time interval corresponding to a year in the real time scale is presented by the ratio of $x = 1.8$ to n_c – the number of years at the optimum cutting age t_o in the real time scale. Since the content of carbon is proportional to the amount of acquired biomass, the obtained annual portions of biomass and carbon uptake are the same for either one – the total uptake of biomass or the carbon content by the cutting age taken as the unit.

Under such assumptions the equity

$$\sum_{n=1}^{n_c} \Delta S_n = \int_0^{x_c} dx \cdot S(x), \quad (10)$$

holds exact for any n_c.

3. RESULTS AND DISCUSSION

The annual uptake at consecutive ages of growing natural forest stands as portions of accumulated stock follows the rate of growth curve (curve 1, Fig. 1). On the other hand, it also depends on the normalised time interval Δx corresponding to real time span of a year expressed by the ratio

$$\Delta x = \frac{x_c}{n_c}. \quad (11)$$

In (11), the cutting age – the number of years n_c the stand has grown before felling in the real time scale and the corresponding normalised time x_c can be chosen arbitrary. For further convenience it is reasonable to choose the cutting age at the maximum of the mean annual increment (curve 2, Fig. 1) corresponding to $x_o = 1.81$ being the optimum age for harvesting at the maximum of land productivity. In that case, (11) transforms into

$$\Delta x = \frac{const}{n_c} \quad (12)$$

the constant being equal to 1.81.

From (12) it follows that logarithm of Δx is a linear function of the logarithm of n_c. Since the current annual increment ΔS_x at a fixed value of $x = const$ is proportional to Δx, it can be found for any n_c from a linear equation

$$log\Delta S_x = A + B \cdot log(n_c). \tag{13}$$

Fractions ΔS_x for $x = 0.9$ close to the maximum rate of growth (Fig. 1) calculated for selected n_c as

$$\Delta S_{0.9} = \frac{S(0.9+\Delta x/2) - S(0.9-\Delta x/2)}{S_o} \tag{14}$$

are listed in Table 1. The plot of $log(\Delta S)$ vs. $log(n_c)$ is presented in Fig. 2. The two data sets fit (13) with correlation equal to 1.0000 and values of coefficients: $A = 0.08648$, $B = -0.9981$. The calculation shows why fast-growing species are more efficient absorbers of atmospheric CO_2 and, therefore, more preferable for the purpose.

Burning wood harvested from an overgrown stand at the age of $x > 1.8$ instead of choosing the cutting age at the maximum of the mean annual increment releases more CO_2 and reduces proportions of the annual uptake with respect to the amount released. Thus, the annual uptake of CO_2 at the age of $x = 0.9$ (14) comprises 0.061 of the amount released by burning wood harvested at $x = 1.8$ from 20 years old stand, while being equal to merely 0.043 of the amount accumulated by a 30 years old stand. It means that instead of 16 ha of 10 years old stands to absorb within a year the amount of CO_2 released by burning wood harvested from 1 ha of 20 years old stand it will take 23 ha to absorb the amount of CO_2 released by burning the harvest from 1 ha of a 30 years old stand. Or, to do the same – a 30 ha plantation of stands of consecutive ages up to 30 years instead of 20 ha plantation of sequentially aged stands up to 20 years. Land productivity in the latter case is by 6.5 % higher.

Table 1.
Annual biomass uptake ΔS at $x = 0.9$ as proportion of the stock accumulated by optimum cutting age $n_c = t_o$

cutting age n_c	Δx	ΔS	$log(n_c)$	$log(\Delta S)$
18	0.1000	0.067822	1.2553	-1.1686
20	0.0900	0.061046	1.3010	-1.2143
30	0.0600	0.040706	1.4771	-1.3903
40	0.0450	0.030532	1.6021	-1.5152
50	0.0360	0.024426	1.6990	-1.6121
60	0.0300	0.020356	1.7782	-1.6913
72	0.0250	0.016963	1.8573	-1.7705
80	0,0225	0.015267	1.9031	-1.8162
90	0.0200	0.013571	1.9542	-1.8674
100	0.0180	0.012214	2.0000	-1.9131
120	0.0150	0.010178	2.0792	-1.9923
150	0.0120	0.008143	2.1761	-2.0892
180	0.0100	0.006786	2.2553	-2.1684
200	0.0090	0.006107	2.3010	-2.2142

The absolute numbers are found from the amount of wood harvested at a certain age in each particular case. Not all the data are always available. However, the average data of annual biomass accumulation can be used for a rough estimate of the limits of CO_2 neutrality. Thus, for instance, according to 2008 forest inventory data [15] the average annual increment of wood biomass in Latvia comprises 834 400 m^3, which is the ultimate amount of firewood that can be used within the limits of CO_2 neutrality no matter where in the world

the firewood produced in Latvia is burnt.

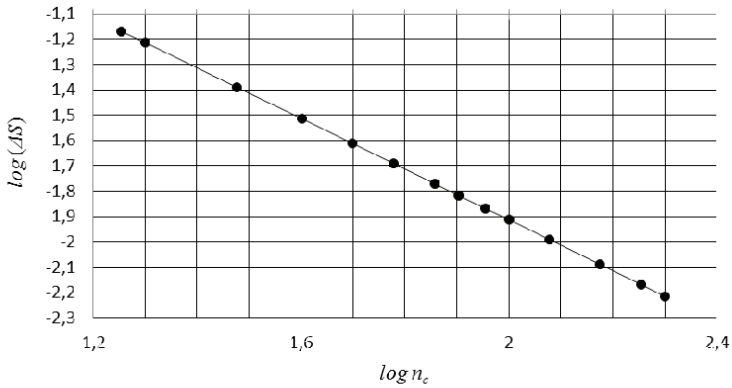

Fig. 2. Annual uptake of biomass ΔS at normalised age $x = 0.9$ as function of the number of years n_c by optimum cutting age at $x = 1.81$.

Considering a bigger picture, the global growing forest and everything made of wood are a deposit of carbon as much as coal or oil, and replacing the two latter by wood just cannot be CO_2 neutral under circumstances of shrinking area of the global forest. The evidence of it is found in the increasing atmospheric concentration of CO_2 despite the enormous quantity of wood from Canadian forest being used to produce electricity since 2008 [4].

Since the biomass (and CO_2) stored in a stand by the cutting age is accumulated in a sequence of years at successive ages, the annual uptake by a plantation comprised of sequentially aged stands (up to the cutting age) of the same size is equal to the stock felled at the cutting age. Consequently, the annual uptake of CO_2 by the plantation is equal to the amount of CO_2 stored in the stand by the cutting age and released at burning of the harvested wood biomass. Therefore, such plantation simultaneously provides sustainable supply of wood to be burned and CO_2 neutrality.

Fast-growing species are preferable for higher biomass productivity and more efficient uptake of CO_2.

The forest area necessary to neutralise the amount of CO_2 released by burning biofuels can be considered the "footprint" of using biomass as the source of primary energy. If CO_2 neutrality is defined by equality of annual amounts released and recaptured, then the area under plantation generating the relevant amount of new biomass is the "footprint" of using fuelwood provided the area is occupied by photosynthesisers to perform the work.

4. CONCLUSIONS

In general, the growing forest functions as a deposit of carbon (along with organic fossil fuels) and as a sink of atmospheric CO_2 pollution, the annual uptake of CO_2 by unit area of a forest stand, amid a number of factors, being dependent on its age.

CO_2-neutrality of fuel-wood is not granted and emissions of CO_2 from burning wood have to be accounted for in the total balance of pollution. On the global scale,

under a shrinking area of the global forest using wood to substitute fossil fuels does not reduce emissions of greenhouse gases.

On the local scale, CO_2-neutrality of biomass fuels is achieved by sustainable harvesting and rotation practices of the fast-growing species being more preferable for sequestration of the atmospheric CO_2 to maintain neutrality.

Sustainable harvesting of wood (and biomass in general) for energy under conditions of limited land assets is incompatible with unrestricted profit-driven economic growth.

ACKNOWLEDGEMENTS

The study has been performed within the agenda of the Latvian National Research Program "Forest and Earth Renewable Resources: Research and Sustainable Utilisation – New Products and Technologies."

REFERENCES

1. Demirbas, A. (2004). Combustion characteristics of different biomass fuels. *Progress in Energy and Combustion Science 30*, 219–230.
2. Goldemberg, J., and Coelho, S. T. (2004). Renewable energy—Traditional biomass vs. modern biomass. *Energy Policy 32*, 711–714.
3. Omri, A., and Nguyen, D. K. (2014). On the determinants of renewable energy consumption: International evidence. *Energy 72*, 554–560.
4. Fuelling a Biomess. (2011). Available at http://www.greenpeace.org/canada/en/recent/Burning-trees-for-energy-puts-Canadian-forests-and-climate-at-risk-Greenpeace/.
5. Brewer, J. (2008). *The coming biofuels disaster.* Available at https://web.archive.org/web/20081025185709/http://www.rockridgeinstitute.org/research/rockridge/coming-biofuels-disaster.html
6. Redman, J., and Tricarico, A. (2013). Wall Street's climate finance bonanza. *Foreign Policy in Focus*. Available at http://fpif.org/wall_streets_climate_finance_bonanza/
7. Searchinger, T. D. et al. (2009). Fixing a critical climate accounting error. *Science 326*, 527–528.
8. Mitchell, S. R., Harmon, M. E., and O'Connell, K. E. B. (2012). Carbon debt and carbon sequestration parity in forest bioenergy production. *GCB Bioenergy 4*, 818–827.
9. Pingoud, K., Ekholm, T., Soimakallio, S., and Helin, T. (2015). Carbon balance indicator for forest bioenergy scenarios. *GCB Bioenergy*. doi: 10.1111/gcbb.12253.
10. Timmons, D. S., Buchholz, T., and Veeneman, C. H. (2015). Forest biomass energy: Assessing atmospheric carbon impacts by discounting future carbon flows. *GCB Bioenergy*, doi: 10.1111/gcbb.12276.
11. Upton, J. (2015). *Pulp Fiction*. Available at http://reports.climatecentral.org/pulp-fiction/1/
12. Abolins, J., and Gravitis, J. (2011). Potential of photosynthesis as a renewable source of energy and materials. *Latv. J. Phys. Tec. Sci. 47* (5), 16–23.
13. Abolins, J., and Gravitis, J. (2011). A simple analytical model for remote assessment of the dynamics of biomass accumulation. *Progress in Biomass and Bioenergy Production*, ed. S. Shahid Shaukat (pp. 91–106). InTech Open Access Publishers. ISBN 978-953-307-491-7. Available at http://www.intechweb.org/booksprocess/aboutthebook/chapter/14232/book/460.

14. Zeide, B. (2004). Intrinsic units in growth modelling. *Ecological Modelling 175*, 249–259.
15. Latvijas Valsts mežzinātnes institūts "Silava". Available at http://www.silava.lv/23/section.aspx/View/119.
16. Schulze, E.-D., Körner, C., Law, B.E., Haberl, H., and Luyssaert, S. (2012) Large-scale bioenergy from additional harvest of forest biomass is neither sustainable nor greenhouse gas neutral. *GCB Bioenergy*, 4 (6), 611–616.

KOKSNES KURINĀMĀ CO_2-NEITRALITĀTES IEROBEŽOJUMI

J. Āboliņš, J. Grāvītis

K o p s a v i l k u m s

Pretēji loģiskam un labi zināmam secinājumam, ka, sadedzinot koksni, atbrīvojas tajā uzkrātais ogleklis, vēl arvien pastāv uzskats, ka biomasa (koksne) neatkarīgi ne no kā ir CO_2-neitrāls reģeneratīvs enerģijas resurss [1-3]. Tikai pavisam nesen [8-10] publikācijās atkal tiek atzīts, ka būtu jāņem vērā oglekļa parāds, kas veidojas starp kurināmā sadedzināšanas brīdi un brīdi, kad atbrīvotais ogleklis no jauna absorbējas biomasā [4-7, 11].

Piedāvātajā pētījumā autori par CO_2-neitralitātes kritēriju izvirza līdzsvaru starp gada laikā atbrīvotā un piesaistītā oglekļa daudzumu. Izmantojot labi pazīstamo empīrisko biomasas akumulācijas Ričardsa vienādojumu (5) [14] izdodas samērā uzskatāmi parādīt biomasas akumulācijas dinamiku atkarībā no audzes vecuma (1. att.) [13]. Tekošo biomasas vai oglekļa gada uzkrājumu dabiskajās audzēs atkarībā no audzes vecuma raksturo līkne **1** 1. att., attiecībā pret kuras maksimālo vērtību normalizētas augšanas ātruma (krājas tekošā gada pieauguma) vērtības laika skalā, kurā par laika vienību pieņemts audzes vecums, kad tā sasniedz maksimālo augšanas ātrumu. Šajā bezdimensiju (normalizētā) laika skalā x audze sasniedz optimālo (produktivitātes – vidējā gada pieauguma, maksimālajai vērtībai atbilstošo) ciršanas vecumu (un optimālo krāju S_o) pie $x = 1{,}81$. Attiecībā pret šo vērtību tekošais krājas gada pieaugums ΔS vecumā $x = 0{,}9$ ((9)) aprēķināts atkarībā no gadu skaita n_c, kad audze sasniedz optimālo ciršanas vecumu 1.tabula, 2. att.).

Kurināmās koksnes CO_2-neitralitāti automātiski nodrošina plantācija, kas sastāv no vienāda lieluma zemes gabaliem ar audzēm secīgā vecumā no viena gada līdz n_c gadiem, katru gadu izcērtot un atjaunojot pa vienam, tādējādi nodrošinot pastāvīgu ikgadēju koksnes produkciju neierobežotā laikā. Piemērotākas enerģijas iegūšanai (un atmosfēras CO_2 piesaistei) ir ātraudzīgās sugas.

Mežs kā oglekļa depozīts pielīdzināms fosilajiem enerģijas nesējiem un koksnes sadedzināšanas rezultātā radītais CO_2 piesārņojums ir iekļaujams kopējā piesārņojuma bilancē, bet fosilo enerģijas nesēju aizstāšana ar koksni nekādā gadījuma nesamazina CO_2 izmešu apjomu. Globālā mērogā, samazinoties kopējai augoša meža platībai, koksnes izmantošana enerģijas iegūšanai nav CO_2-neitrāla.

Ilgtspējīga koksnes izmantošana enerģijas vajadzībām nav savienojama ar neierobežotu ekonomisku izaugsmi peļņas gūšanai.

02.06.2016.

LATVIAN JOURNAL OF PHYSICS AND TECHNICAL SCIENCES
2016, N 4

DOI: 10.1515/lpts-2016-0029

SCENARIO ANALYSIS FOR FUTURE OIL DEMAND AND SUPPLY ON THE HORIZON OF 2022

Hasan Mustafa

Finance and Economics Department Business Administration College
University of Sharjah
P.O. Box 27272 Sharjah
United Arab Emirates
e-mail: hmustafa@sharjah.ac.ae

This study indicates signs of recovery in the oil price beyond 2020 and predicts oil prices will reach $80 in 2022. This scenario posits an opposite view to a large number of experts who believe that oil prices will remain low for a long time. The second less preferred scenario predicts oil prices of $60 in 2022 due to a big spread in shale oil production technology worldwide, combined with a significant increase in oil production costs.

Keywords: *conventional oil, oil demand, oil price, oil supply, unconventional oil.*

1. INTRODUCTION

Global oil consumption increases significantly each year. The transportation sector, as well as urbanisation and the increase in the standard of living will be the main forces of oil consumption in the future, especially in developing countries. The increase in the global population also has a crucial impact on the growth of future oil demand. The strong rise in unconventional oil production was the main driver for a recent oil supply glut, which has caused a huge oil price fall since July 2014. This paper emphasises conventional oil depletion in different areas worldwide as well as limitations on unconventional oil production in North America by analysing two different scenarios for future oil prices in 2022.

2. METHODOLOGY

This paper uses scenario analysis to estimate the future oil price in 2022. This is an important tool in the world of finance and economics to make projections for the future. Scenario analysis is a process of analysing possible future events by considering alternative outcomes. As the main method of economic projection, scenario analysis presents several alternative future developments and does not try to analyse

only one exact picture of the future [1]. Unlike forecasts, it does not extrapolate from the past; historical data are not expected to outline future projections. Rather, it takes into account possible developments and turning points connected to the past. Through the development and use of scenarios, we challenge our expectations and are better prepared for the unexpected outcome, when it occurs.

Purpose of the research: This paper aims to describe two scenarios for future oil prices based on future oil demand and supply in 2022 and evaluate the preferred and more probable scenario depending on different factors of supply and demand.

3. RESEARCH AND DISCUSSION

3.1 Future Oil Demand by 2022

The significant key drivers for future oil demand growth are the rising world population, rapid urbanisation, the increase in the living standard (especially in developing countries), and the transportation sector. This last driver is the most important key driver for oil demand growth in the future.

According to the United Nation Department of Economics, the world population is expected to reach 7349 million at the end of 2015 and 8501 million in 2030 [2]. Based on this estimation and current growth trends, the world population is expected to increase about 8 % (around 83 million each year) and reach 7930 million in 2022. The rise appears mainly in developing countries in Asia, Africa, Latin America, and the Middle East. By 2022, the population of India will surpass that of China to become the largest populated country.

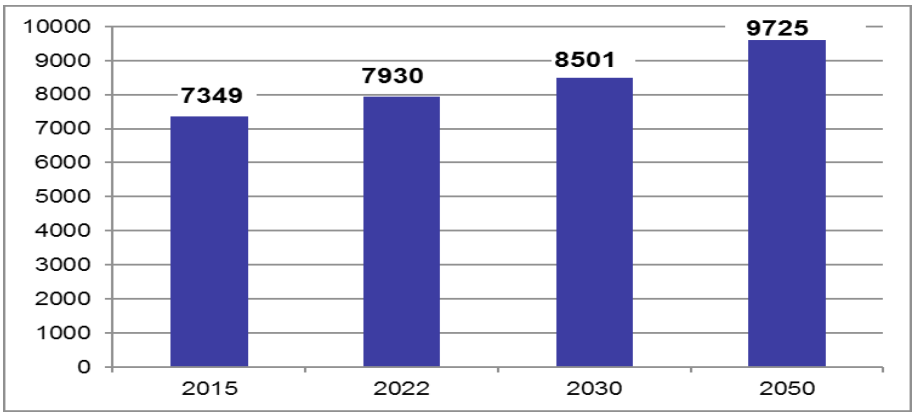

Fig. 1. Expected future world population.

Urbanisation will have very important implications in terms of future oil consumption, since the lifestyle (including vehicle ownership patterns as well as vehicle miles travelled) is closely linked to urbanisation trends. Nowadays, there are more people living in urban areas than in rural areas. The United Nations forecasts that about 54 % of the world's population in 2014 [3] is living in urban areas and estimates that the world's urban population will increase to reach 66 % in 2050. Based on this estimation, the world's urban population is expected to rise respectively to

reach 57 % in 2022. This trend will be stronger in developing countries, especially in Asia and Africa. Worldwide, around 550 million more people will live in urban areas by 2022, in comparison with 2015.

Increases in the living standard in developing countries where economic growth is expected to be above 6 % on average in China and India in the next five years [4] will lead to rapid increases in oil consumption per person in 2022. This trend will appear very strongly in China, India, and Indonesia. Oil demand is rising as hundreds of millions of people in China, India, Indonesia, and other developing countries move out of poverty and turn to a modern lifestyle using increasingly more fuel based transportation.

India and China have increased their oil consumption rapidly in recent years. This trend will continue in the future. Annual oil consumption per capita in China and India is expected to increase very strongly by about 30 % from expected 2.9 and 1.3 barrels/year in 2015 to reach around 3.8 and 1.7 barrels/year in 2022. Whereas in the USA, oil consumption per person is 22.2 barrels/year and this level will remain almost the same in the next seven years. China and India still have a huge gap to fill before reaching the world average of about five barrels/year.[1]

The importance of the transportation sector to future oil demand growth appears huge. From demand growth due to social mobility in developing countries, especially in China, and India, there are also growing numbers of automobile users as well as a fast-growing demand for air transport in recent years. This trend will continue in the future.

The transportation sector is a significant key driver of future oil demand growth. On the one hand, the total number of passenger cars is expected to increase rapidly in 2022 by around 260 million (about 23 %) to reach 1.4 billion. This growth will appear prominently in developing countries, with around 200 million cars more over this period of time. The number of heavy and commercial vehicles is also expected to increase strongly (about 24 %) to reach almost 290 million by 2022.[2] The main influence for this growth will be developing countries. On the other hand, efficiency improvements, the use of alternative fuels such as biofuel, and the adoption of non-oil-based engines, tend to be limited. The number of electric cars reached one million in 2015 worldwide and the potential for this market will be limited in the near future. Thus, the possibility of switching from oil-based engines to battery electric cars will be only visible in the long term, perhaps after 2030.

International tourist arrival is expected to reach almost 1.5 billion in 2022; about 26 % more compared with the expected estimate of 1.185 billion in 2015[5]. This will be a very important indicator for future oil demand growth. In this regard, Airbus Group is expecting a new demand for 32,600 airplanes in the next 20 years [6]: about 13,100 for replacement and 19,500 increasing from 19,000 at the beginning of 2015 to reach 38,500 in 2034. That means the number of airplanes is

[1] Based on the worldwide average for oil consumption about 96 million barrel / day and world population 7349 million.

[2] This expectation for the reference year 2022 based on different estimations for the total current number of passenger cars and heavy commercial vehicles as well as the potential growth in the future.

expected to increase by about 8,000 to reach 27,000 at the end of 2022 and that will lead to an increase in the oil demand for the aviation sector from the expected 5.5 in 2015 to7 million barrels per day in 2022.

Our previous experience with various estimations from different international authorities proved, in most cases, to underestimate the future oil demand. The previous estimation in World Oil Outlook from Organization of the Petroleum Exporting Countries OPEC in 2013 for oil demand in 2015 was 91.6 million barrel/day. However, nowadays the current estimation for 2015 is about 92.88 million barrel/day, which is 1.22 million barrels a day higher than previous estimation by the Organization of the Petroleum Exporting Countries OPEC. International Energy Agency (IEA) estimates oil demand about 94.54 million barrel/day on the average and U.S. Energy Information Administration around 93.82 million barrel/day. Based on these estimations from the three different international authorities, oil demand is expected to be about 93.75 million barrel/day in 2015. Taking into consideration the effects of all key drivers of oil demand growth in the future and the assumption for no ambiguity on the demand side in the next seven years, only one scenario will be considered for oil demand in 2022. In this scenario the oil demand is expected to increase about 8 million barrel/day over the time period of 2015–2022, reaching around 102 million barrel/day in 2022. The big question will still remain: are we going to have enough oil supply to satisfy the increase in oil demand?

3.2 Future Oil Supply by 2022

Conventional oil:

The production of conventional oil has remained essentially flat in recent years, while there has been growth in unconventional oil usage in North America. I believe this is the general belief of most experts, but let us consider the ideas of others, who say we have not reached the peak (the concept of limitations on conventional oil production) yet. But that does not mean we are very far from reaching the peak; if we have not reached the peak yet, we will definitely reach the peak very soon.

The existing conventional oil fields are being depleted in increasing numbers of regions worldwide; in the next two decades, without replacement of old fields in depletion areas where constant drilling of new wells are necessary, the global conventional oil production will quickly shrink. In order to keep the oil flowing in the last decade, the oil companies worldwide have invested more than 4 trillion $ for oil drilling. Around $2.5 trillion of this was spent on replacing production from existing exhausted oil fields [7].

The investment in oil production is expected to decrease about 20 % in 2015 [8] as well as in 2016 because of strongly decreasing oil prices by about 70 % in the last 15 months. Wood Mackenzie energy consultancy said that low oil prices were forcing companies to cancel projects worth $170 billion which had been planned to be implemented between 2016 and 2020 [9]. In addition, the cost of capital is expected to increase in the near future after the first step since 10 years to increase the discount rate with 0.25 % in the USA in December 2015. Investments in oil

production in the future are going down, which can lead to significant stagnation or limitation in the oil supply in the coming few years. This will tend to limit the ability to increase the conventional oil production in the period of time 2020–2022. The international oil companies have reached their limits; their profits fell rapidly in 2015. Costs for finding and developing new oil fields have tripled since 2005 and the return from these costs has not been enough to cover the costs in 2015 in some cases. Most international oil companies have announced significant reductions in their exploration and drilling programmes in the next few years [10].

Oil fields have similar lifecycles. Upon drilling a well, oil is increasingly extracted until it reaches its optimal production after which it declines due to depleting oil stocks. Technological innovations can extend well life, but depletion is inevitable [11].

The business of estimating oil reserves is controversial and political; most official figures are unreliable. Estimating reserves is a huge challenge; there is a range of genuine uncertainty as well as political manipulations to consider. The discovery of new conventional oil fields has been nearly exhausted in recent years and is expected to be dramatically limited in the future. Based on that assumption, there will be no new discovery for conventional oil in the coming few years. From this we can estimate the time frame for oil depletion in many countries worldwide.[3]

Table 1

Expected Oil Depletion in Many Countries Worldwide

Country	Proven conventional oil reserve in billion barrel	Production of conventional oil in million barrel / day	Oil consumption in million barrel / day	Estimated time frame for oil depletion
UAS [1]	30	5	19.5	2030–2032
China	25	4.6	11	2028–2030
Brazil [2]	15	3	3	2028–2030
Algeria	12	1.7	0.42	2033–2035
Mexico	10	2.8	2	2025–2027
Angola	10	1.75	0.12	2030–2032
Azerbaijan	7	0.9	0.1	2035–2037
India	5.7	1	4	2030–2032
Norway	5.5	1.9	0.22	2023–2025
Oman	5.5	1	0.175	2031–2033
Egypt	4.5	0.7	0.8	2030–2032
Malaysia	4	0.7	0.7	2030–2032
Indonesia	3.7	0.9	1.8	2027–2029
UK	3	0.9	1.5	2025–2027
Argentinian	2.4	0.7	0.8	2025–2027

If we consider the fact that oil will dry up in many areas in the next two decades and there will be redistribution in oil supply, most oil supply in the future will be coming from certain and limited geographical areas. That will dictate a great geopolitical challenge as well as a potential risk for oil supply.

[3] These expectations are based on various estimations and different sources of data for 2015.

The major technical modalities of alternative energies (solar and wind energy) face great challenges in respect to being intermittent in nature. Furthermore, we are still lacking the technology to properly store energy.

Considering the fact that we had only a slight increase in investment in the last two years in the alternative energy field, investment in the alternative energy on a large scale needs a political decision, which in most instances lacks popularity.

The importance of the transportation sector, which accounts nowadays for about 58 % of oil consumption worldwide, to future oil demand growth appears largely from demand growth in mobility and the limited fuel switching possibilities. In the next seven years the potential to switch from fuel based engine to electric battery cars will be limited; the total global sales of electric vehicles will be about 500,000, whereas global vehicle sales are projected to reach approximately 89 million units in 2015.

The total number of electric cars is expected in a best case scenario to reach 20 million in 2020 [12] less than 1.5 % of all passenger cars. The adoption of non-oil-based engines will develop strongly in the long term especially beyond 2030.

Unconventional oil:

The highest potential for additional biofuels exists in the US, Europe, and Brazil. The biofuel supply in the medium-term will rise from an expected two barrel/day in 2015 to about 2.7 in 2022. In a long term scenario, it will reach almost 5 million barrel / day in 2035 [13]. Biofuels will remain costly, limited, and may be developed at the expanse of feeding people.

Initial estimations for shale oils were amazing and surprising, but nowadays the current estimations have been slimmed down. About $400 billion [14] has been used to drill shale oil and gas wells in the US, and increase oil sands production in Canada since 2009. North American unconventional oil production constitutes nearly all the growth in oil supply worldwide in recent years.

Tight oil supply from US & Canada is expected to plateau by 2019/2020 [13]. Many experts opine that the tight oil reserves are close to being exhausted and that more expensive unconventional oil reserves such as shale oil and heavy oil, deep-water oil as well as renewable energy sources may need to be exploited.

US production of tight oil production fluctuates in the short term but will register an upward trend as prices recover and technologies improve [8]. US tight oil output is predicted to reach a plateau in 2020, just about 5 million barrel /day, before starting a gradual decline.

Over the past six years, unconventional oil production has undergone a revolution especially in North America with significant increases in production from oil sands in Canada, tight oil, and shale oil in the US. The US has been the main driver of crude production growth recently. Hydraulic fracturing and horizontal drilling technology have enabled large scale extraction to shale oil at relatively economic costs leading to a growth in global oil production [15].

Just 18 months ago, a barrel of crude oil was around US$110. Nowadays the same barrel of oil is trading for less than $30, with oil prices lower than $30 it be-

comes increasingly harder for higher cost shale oil producers to compete with low-cost producers such as those in the Gulf region.

Shale oil production is more complex and expensive than conventional oil production. The International Energy Agency supposes maintaining production at one million barrels per day. The Bakken shale oil field requires 2,500 new wells a year; a large conventional field in southern Iraq needs just 60 [16]. According to a new analysis by Moody's Credit Rating Agency, the median North American shale oil producer needs $42 per barrel to cover costs [17], in contrast the cost for conventional oil in the Gulf region is about $13 per barrel, such as Ghawar giant oil field in Saudi Arabia with around 5,000,000 oil barrels output per day, Burgan field in Kuwait with 1,700,000 barrel/day, and Rumaila field in Iraq with 1,300,000 barrel/day. The shale oil industry cannot survive on $30 oil prices, whereas the Middle East could still gain significant profits.

Lower oil prices have huge implications in the shale oil industry, while production efficiency advancements, which include maximising initial production rates, improving ultimate recovery from each new well, reducing average drilling costs and accelerating drilling time over the past 18 months have pushed down the break-even prices to be as low as $30 for some US shale producers, in the best areas of already existing oil fields, and significant decreasing of the marginal cost from about $ 70 two years ago to less than $50 today on the average.

The low price of crude oil has cut the number of drilling rigs in the United States by almost two-thirds, from 1,600 to almost 500 [18]. Shale drilling is becoming more efficient and less expensive due to benefits from improvements in technology.

Nowadays, lower oil prices have a negative impact on shale oil investor portfolios. In recent years, it has still been relatively easy for shale oil producers in the US to raise capital by selling debt or equities, in spite of the past 18 months' oil price crash caused by a global oil supply glut. At the beginning of 2016, this crash decreased revenue significantly, which currently means some shale oil producers are operating at a loss. Also, the cost of capital has increased gradually after the US Federal Reserve started to raise interest rates. Since December 2015, the amount of debt held by US oil and gas producers has climbed to slightly more than $200 billion in 2015 [19]. As a consequence, some shale oil producers have seen a huge reduction of their debt rating and are now facing difficulty obtaining financing and face looming bankruptcy. Capital is starting to dry up for US shale oil producers or become distinctly costly, which leads to roughly about a 20 % expected reduction in investment in shale oil industry in 2016 and 2017.

This situation will probably force some shale oil producers to leave the market, which means the US total oil production is expected to decrease by about 700,000 barrel a day on the average in 2016. The U.S. Energy Information Administration (EIA) said in a forecast released recently that U.S. oil production peaked at 9.7 million barrels a day last April 2015, the highest level since 1971. U.S. crude oil production is expected to decrease from an average of 9.4 million in 2015 to 8.7 million in 2016, and is projected to bottom out at 8.5 million barrels a day in 2017 [20].

The production of shale oil damages the environment and does not ensure

security for oil supply in the long term. The Natural Resources Defence Council (NRDC) warns about the danger of shale oil production. The study explores the potential environmental impact of extracting shale oil [21], and makes reference to environmental damage in the water resources [22] as well as in the agriculture sector caused by the chemicals used in the shale oil production. In addition to environmental implications of shale oil production, the big question will remain in the future, whether it makes sense to extract shale oil resources as a substitute for the depleting of conventional oil. Nowadays, there is a huge debate in the US about the environmental damage caused by shale oil production, which will probably limit the spread of shale oil production nationwide or abroad.

Scenario I:

Global supply of oil is currently expected to be about 1.5 million barrels per day on average. The expected decline in the total US oil production in 2016 and probably also the decline in non-OPEC oil production in the coming two years as a result of the crash in oil prices (as well as the huge reduction in investment) will eliminate the current oil supply glut in 2017/2018, and lead, probably, to a shortage in oil supply beyond 2020 as the demand increases strongly in developing countries such as China, India, and Indonesia.

According to most forecasters, global oil demand is growing annually more than 1 million barrels a day on the average in the next seven years reaching about 102 million barrel a day in 2022, which must be met from an increase in supply somewhere. According to the EIA ("Short-Term Energy Outlook", August 2015), US oil production has held up surprisingly well in the face of a fall in prices, but is expected to be lower at the end of both 2015 and 2016 than at the end of 2014.

Rising interest rates as well as a wave of expected bankruptcies will increase the cost of capital; decreasing conventional oil production by non-OPEC producers such as in the North Sea and Gulf of Mexico and increasingly shift to expensive oil such as shale and deep-water oil to replace depleting fields. This will increase the marginal cost of production. In addition, shale oil production will not be able to compensate for the expected decline in US conventional oil production beyond 2020, so most oil supply in the future will be coming from geographically limited areas, mainly the Middle East, Venezuela, and Russia. However, the estimates for the future oil supply have not taken into consideration the potential of future geopolitical challenges which seem inevitable. We are just seeing now the changes in East Europe and the ongoing turmoil in the Middle East. Taking into consideration the turmoil in these regions, which is expected to continue in the future and adding risk premium for probable disturbances in future oil supply to future oil prices, we come up with the following first scenario:

Expected preferred scenario for oil price is to fluctuate around $ 80 in 2022.

Scenario II:

The second scenario is based on the following two positive assumptions for oil supply: 1. significant growth in conventional oil production outside as well as inside Organization of the Petroleum Exporting Countries (OPEC) will continue. 2. The continuation of techniques pioneered for shale oil production to other areas in

the United States and abroad to countries such as China, Russia, and Argentina. In places other than the US and Organization of the Petroleum Exporting Countries, growing oil production requires major investment to offset decline rates from existing wells and add extra output. Taking into consideration the expected rise of the cost of capital in the near future as well as the expected increase in the marginal cost as a negative factor for an increase in oil production cost will lead to the following second scenario:

Expected less preferred scenario for oil price is to fluctuate around $60 in 2022.

4. CONCLUSION

This study revealed two possible scenarios for future oil prices based on the analysis of expected future oil demand and supply in 2022, taking into consideration, on the one hand, the depletion of conventional oil supply in some geographical areas worldwide; and on the other, the potential and limitations of the unconventional oil supply, especially in North America. Oil is a limited resource, and the remaining accessible reserves are consumed more rapidly each year. Remaining reserves are increasingly more technically difficult to extract and therefore more expensive.

The depletion of conventional oil in different areas worldwide and the limitation on the unconventional oil production due to environmental damage, the higher cost of production and the expected reduction in investment in oil sector worldwide in the coming few years will lead to the elimination of the oil supply glut by 2018. This will stabilise the oil market for some time and lead to a significant recovery of oil prices in 2022. Future extraction of oil reserves will be extremely costly.

REFERENCES

1. Chermack, T., Lynham, S. A., and Ruona, W. (2001). A review of scenario planning literature. *Futures Research Quarterly*, 17(2).
2. United Nations. (2015).World Population Prospects: The 2015 Revision.
3. United Nations. (2014).World Urbanization Prospects: The 2014 Revision.
4. International Monetary Fund. (October, 2015). World Economic Outlook Database.
5. World Tourism Organization. (2014). *Annual Report*.
6. Airbus. (2015). *Global Market Forecast 2015–2034*.
7. Kopits, S. (2014). *Oil and Economic Growth. A Supply-Constrained View.* Available at http://energypolicy.columbia.edu/sites/default/files/energy/Kopits%20-%20Oil%20and%20Economic%20Growth%20%28SIPA,%202014%29%20-%20Presentation%20Version[1].pdf
8. OECD/IEA. (2015). *World Energy Outlook 2015, Executive Summary, International Energy Agency*. Available at https://www.iea.org/Textbase/npsum/WEO2015SUM.pdf
9. Krishnan, B., and Bousso, R. (2016). *Oil up 7 Percent as Iran Welcomes Output Freeze without Word on Cuts.* Reuters. Availabe at http://www.reuters.com/article/us-oil-production-cuts-idUSKCN0US06W20160114.
10. Tippee, B., and Xu, C. (2015). Companies slash capital budgets as oil price drop cuts cash flows. *Oil & Gas Journal*, 113(4), 28-+.

11. Energy Reality. Available at http://energy-reality.org/peak-oil-and-resource-depletion/
12. Trigg, T., Telleen, P., Boyd, R., Cuenot, F., D'Ambrosio, D., Gaghen, R., and Kaneko, H. (2013). Global EV outlook: Understanding the electric vehicle landscape to 2020. *Int. Energy Agency*, 1–40.
13. World Oil Outlook. (2013). *Organization of the Petroleum Exporting Countries*. OPEC Secretariat, pp. 12–134.
14. Urbanomics. *Oil Industry – This Time Is no Different!* (2016). Available at http://gulzar05.blogspot.ae/2016/01/oil-industry-this-time-is-no-different.html
15. International Energy Agency. (2013). *Resources to Reserves, Oil, Gas and Coal Technologies for the Energy Markets of the Future*, pp 63–64.
16. The Economist. (2014). *The Benefits of Shale Oil are Bigger than Many Americans Realise. Policy Has yet to Catch Up.* Available at http://www.economist.com/news/united-states/21596553-benefits-shale-oil-are-bigger-many-americans-realise-policy-has-yet-catch
17. Fuelfix. Available at http://fuelfix.com/blog/2015/08/13/moodys-42-per-barrel-is-enough-to-cover-costs/#30935101=0
18. *North American Rotary Rig Counts*. Available at http://www.wtrg.com/rotaryrigs.html
19. Financial Times. (2016). *Oil: US Shale's Big Squeeze.* Available at http://www.ft.com/intl/cms/s/0/2db96dae-c0eb-11e5-9fdb-87b8d15baec2.html#axzz3yuUkhuYW
20. U.S. Energy Information Administration. (2016). *Short-Term Energy Outlook*. Available at http://www.eia.gov/forecasts/steo/pdf/steo_full.pdf
21. Bordetsky, A., Casey-Lefkowitz, S., Lovaas, D., Martin-Perera, E., Nakagawa, M., Randall, B., and Woynillowicz, D. (2007). *Driving It Home: Choosing the Right Path for Fueling North America's Transportation Future*. Natural Resources Defense Council (United States); Western Resource Advocates (United States); Pembina Institute (United States).
22. Bartis, J. T., LaTourrette, T., Dixon, L., Peterson, D. J., and Cecchine, G. (2005). *Oil Shale Development in the United States: Prospects and Policy Issues.* Rand Corporation.

NAFTAS PIEPRASĪJUMA UN PIEDĀVĀJUMA IESPĒJAMO SCENĀRIJU ANALĪZE LĪDZ 2022. GADAM

H. Mustafa

K o p s a v i l k u m s

Publikācija apkopo autora individuāla pētījuma rezultātus, kas veikts Emirātu Tehnoloģiju koledžā (Abū Dabī, AAE) un Šārdžas Universitātē (Šārdža, AAE). Pirmoreiz pētījums prezentēts „Pasaules tendenču, ideju un biznesa kontaktu forumā" (Rīga, Latvija, 2014. gada 10.–11. aprīlis). Attiecībā uz pirmo vēlamo scenāriju par naftas cenu atveseļošanās pazīmēm pēc 2020. gada, tiek secināts, ka 2022. gadā tās sasniegs 80 ASV dolārus. Šis scenārijs nesakrīt ar daudzu ekspertu viedokli, kuri paredz, ka zemas naftas cenas saglabāsies vēl ilgu laiku. Savukārt otrs, mazāk vēlamais scenārijs paredz naftas cenu celšanos 2022. gadā līdz 60 ASV dolāriem. Tas tiek skaidrots ar iespējamu slānekļa naftas ražošanas tehnoloģiju izplatību visā pasaulē, kas norisinātos vienlaikus ar naftas ražošanas izmaksu pieaugumu.

03.07.2016.

LATVIAN JOURNAL OF PHYSICS AND TECHNICAL SCIENCES
2016, N 4

DOI: 10.1515/lpts-2016-0030

ELECTRONICS

INVESTIGATION ON MAXIMUM AVAILABLE REACH FOR DIFFERENT MODULATION FORMATS IN WDM-PON SYSTEMS

I. Kurbatska, V. Bobrovs, S. Spolitis, P. Gavars, G. Ivanovs, R. Parts

Institute of Telecommunications, Riga Technical University,
12 Azenes Str., LV-1048, Riga, LATVIA
e-mail: inna.kurbatska@rtu.lv

Considering the growing demand for broadband of access networks, in the present paper we investigate various modulation formats as a way of increasing the performance of optical transmission systems. Non-return-to-zero (NRZ) on-off keying, return-to-zero (RZ) OOK, carrier suppressed RZ (CSRZ) OOK, duobinary (DB), NRZ differential phase shift keying (NRZDPSK), RZ-DPSK and CSRZ-DPSK formats are compared using the maximal achievable reach with bit error rate less than 10^{-9} as a criterion. Simulations are performed by using OptSim software tool. It is shown that using the transmission system without dispersion compensation the best results are shown by duobinary and CSRZ-OOK modulation formats, but with the system using dispersion compensating fiber (DCF) the longest transmission distance is achieved by RZ-DPSK modulation format. By investigating the influence of channel spacing for best-performed modulation formats, network reach decrease for transmission systems with DCF fiber has been observed due to channel crosstalk.

Keywords: *carrier suppressed RZ (CSRZ), chromatic dispersion (CD) compensation, dispersion compensating fiber (DCF), duobinary (DB), modulation formats, non–return-to-zero (NRZ), NRZ differential phase shift keying (NRZ DPSK), return-to-zero (RZ), wavelength division multiplexing (WDM).*

1. INTRODUCTION

According to [1] there are three main components of Internet traffic – web data, file sharing, and internet video wherein the percentage of video traffic is growing annually. Different voice services, videoconferencing, telecommuting, distance learning, online e-commerce, always-on communication, the exchange of larger attachments for emails and messaging – all this increases the subscribers' demand for internet broadband [2], [3]. That is why copper technologies based on digital subscriber line (DSL), which have been widely used over the past 10 to 15 years, are not more able to satisfy these demands [4]. For this reason, new solutions should be found for access networks.

Today one of them is widely applied FTTH technology. There are various Fiber to the X (FTTX) solutions, which differ for the different fiber termination points in the optical distribution network (ODN). The performance of Fiber to the Home (FTTH) networks is the best, but they are also the most expensive to implement [5]. FTTH or Fiber to the Building (FTTB) is the leading ultrafast broadband solution and its adoption in Europe is growing (the total number of subscribers increased by 29 % in 2013). By the end of 2013, 34 global and 23 European countries had reached the threshold of more than 1 % of homes directly connected with optical fiber. But only in the nine countries around the world FTTH/B subscribers are more than 20 % of its households [6], [7]. This means that applying of FTTH is still topical.

Although there are several scenarios for FTTH implementation such as passive optical network (PON), active optical network (AON) and point-to-point (P2P) physical link from the central office (CO) to each user, PONs are actually considered the most cost-effective way [5]. That is why PON performance improvement is the aim of our research. There are several PON standards. According to [8] Gigabit-Capable PON (GPON) is currently dominating in the world market, but 10 Gigabit Ethernet-PON (10G - EPON) and 10G-PON (XG-PON) are currently at beginning phase of mass-market adaptation. In 2015 global spending to PON technology was divided in the following way: GPON – 50 %, 10G EPON – 22 %, EPON – 18 %, XG-PON – 12 %.This means that 10 Gbit/s systems are being widely enough introduced now and for this reason we are using this speed in our transmission system simulation. In the roadmap defined by the Full Service Access Network (FSAN) group, describing the evolution of optical access networks in the next years, XG-PON has already been selected as the best candidate for next generation PON1 (NG-PON1) solutions [5]. This is the first phase of NG-PON project. NG-PON1 considers the ODN-compatible systems, and NG-PON2 requires the ODN to be changed [4]. The technology, which can substitute traditionally used TWDM-PON in NG-PON2, is WDM-PON that we consider in the present paper. In WDM-PON signal splitting is carried out using optical wavelength division instead of previously used optical power division.

As mentioned above, the increase of transmission bandwidth is an important task to solve today. One of the ways how to increase the capacity and scalability of transmission system is by using appropriate modulation format [5], [9], [10]. There are three physical attributes that can be used to carry information: intensity, phase (including frequency), and polarization. Respectively, there are four modulation formats – amplitude shift keying (ASK) also known as on-off keying (OOK), phase shift keying (PSK), frequency shift keying (FSK) and polarization shift keying (PolSK). FSK is rarely used for lightwave systems due to complexity involved in recovering the frequency-coded information. Polarization shift keying (PolSK) has also received comparatively little attention for use in WDM-PON access networks due to its complexity [4], [9], [10]. There are also some advanced formats, which are combination of the above-mentioned modulation techniques, for example, quadrature amplitude modulation (QAM), which is the combination of ASK and PSK, where both the phase and amplitude of the carrier are changed at the same time [9].

According to [11] till lately, the dominant optical modulation format in the optical transmission system was non-return-to-zero (NRZ) on-off keying OOK with

direct detection (DD); however, demand on higher data rates, better system reliability and optimal working conditions motivated many studies in this field.

In the present paper, we focus on modulation formats, which may show better performance in comparison with traditionally used NRZ-OOK and are not so difficult to implement as advanced modulation formats such as, for example, QAM or QPSK. For relatively not very high speed as 10 Gbit/s, it is more profitable to use more cost effective solutions if they are able to fulfil the technical network needs. Hence, we compare the maximal reach of systems with NRZ-OOK, RZ-OOK, CSRZ-OOK, DB, NRZ-DPSK, RZ-DPSK and CSRZ-OOK formats. Authors in [12] compare the formats implemented in different network topologies with various splitting ratios and relatively small optical transmission length. The results show that among OOK formats (NRZ, RZ, CSRZ and CRZ) CSRZ and CRZ formats have the lowest BER. Comparing between NRZ, CSRZ and DB, the best performance is demonstrated by CSRZ, followed by DB and finally by NRZ. In comparison with NRZ-DPSK, RZ-DPSK show better performance. Authors in [11] compare NRZ, RZ, CRZ, CSRZ, DB, NRZ-DPSK and RZ-DPSK and the best performance is shown by DB and good results are also demonstrated by NRZ-DPSK. These results are obtained for 8-channel WDM-PON with transmission over 50 km long fiber span. We compare the performance of these formats (excluding CRZ and including CSRZ-DPSK) for 16 channel WDM-PON and longer distances, in addition investigating different channel spacing. Analogical approach is applied in [13], authors demonstrate that using DB format, the signal can be transmitted over 130 km long fiber span by using 25 GHz channel spacing. NRZ-DPSK can be transmitted over 100 km, but RZ-DPSK, CSRZ and NRZ over 70 km. For RZ transmission distance is smaller. DB also showed good results using 12.5 GHz channel spacing. We demonstrate that maximal reach can be even longer using DCF.

Extension of the maximum available reach or the number of end-users (which are conflicting requirements) of a single PON allows consolidating the number of COs and, respectively, the operators' expenses [5]. Hence, we evaluate the maximal transmission distance of system using each modulation format to compare their performance. To find out which modulation format is most appropriate for definite transmission conditions in WDM-PON system, we evaluate their performance with and without dispersion compensation module (DCM). One of the solutions how to increase transmission capacity or spectral efficiency is to reduce the channel spacing [14]. For this reason, different channel spacings are investigated in our WDM-PON research.

We use the OptSim software for our simulations. In OptSim software, signal propagation in the optical fiber transmission system is described solving the nonlinear Schrödinger equation using the Time Domain Split Step (TDSS) technique, which allows simulating linear and nonlinear effects independently of each other [15].

2. SIMULATION MODEL OF WDM-PON TRANSMISSION SYSTEM WITH DIFFERENT MODULATION FORMATS

Our implemented simulation scheme of WDM-PON optical access system is shown in Fig. 1. As typical PON, it consists of three main parts: optical line terminal

(OLT), optical distribution network (ODN) and optical network terminal (ONT). OLT is located at operator's central office (CO) and ensures data exchange among the PON and metro-access or long haul network. ODN performs the transport function and, consequently, includes an optical transmission line. Besides, optical splitters and optical combiners, which are situated at CO and remote node (RN) are also part of ODN. What is important, according to PON principles, all optical equipment placed in ODN should be passive. ONT is situated at user's side and its function is to convert received optical signal to electrical and contrariwise [16].

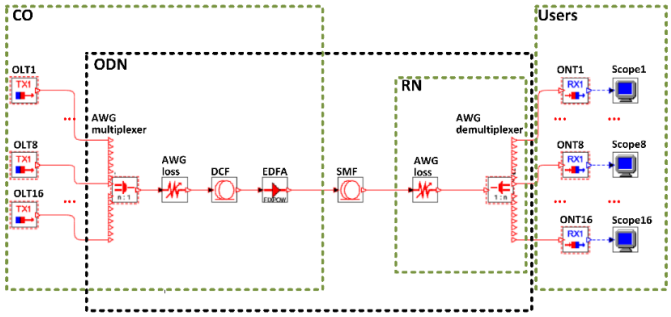

Fig. 1. Simulation scheme of 16-channel WDM-PON transmission system with transmission speed of 10 Gbit/s per channel.

Our WDM-PON system consists of 16 10 Gbit/s channels with 193.1 THz central frequency. The initial channel spacing is 100 GHz and channel frequencies are assigned according to ITU-T G.694.1 recommendation. This recommendation defines the DWDM frequency grid, i.e., the values of central frequencies for the transmission channels [17].

Our simulation model is one-directional and executes data transmission from an operator to a user (download). For this reason, as one can see in Fig. 1, optical transmitter forms OLT and is situated at CO, but ONT is composed of an optical receiver. Each modulation format requires different transmitter structure, but in our simulations all of them are based on CW laser with +2 dBm output power and 50 MHz 3-dB linewidth. Transmitter schemes, which have been used in our case, are shown in Fig. 2 and will be described further. Receivers for all intensity modulation formats and for all phase modulation formats are similar. Receiver for intensity modulated signals is based on PIN photodetector with -22 dBm sensitivity [5], [18]. Receiver, which is used for phase modulated signals, consists of tunable Mach-Zehnder interferometer where optical paths differ by a delay equal to the duration of bit and two PIN photodetectors with responsivity of 0.75 A/W at reference frequency of 1550 nm and 2 nA dark current. Each optical output of interferometer is detected by PIN photodetector. The output electrical signal is the difference between the PIN detected currents [18], [19]. Electrical signals on the output of receivers are filtered using low-pass Bessel electrical filter with bandwidth experimentally chosen as the most appropriate for each modulation type.

In our simulation model, we use arrayed waveguide grating (AWG) based multiplexer for channel combining. For dispersion compensation, dispersion compensation fiber (DCF) is used [20]. AWG together with DCF and erbium-doped fi-

ber amplifier (EDFA) is placed at CO. DCF is used only in the second simulation scenario, for the research of WDM-PON systems without dispersion compensation. EDFA used in our simulations has fixed output power equal to +16 dBm. The key parameters of DCF fiber are attenuation coefficient α = 0.6 dB/km, dispersion coefficient D= -80 ps /(nm·km) and dispersion slope D_{sl}= 0.19 ps/(nm2·km). The standard ITU-T G.652 single mode fiber (SMF) is used as the optical transmission line. AWG demultiplexer, which is situated at remote node (RN), is used for signal splitting and filtering. The insertion loss of both AWG multiplexers and demultiplexers is equal to 3 dB and is simulated by using additional optical attenuators.

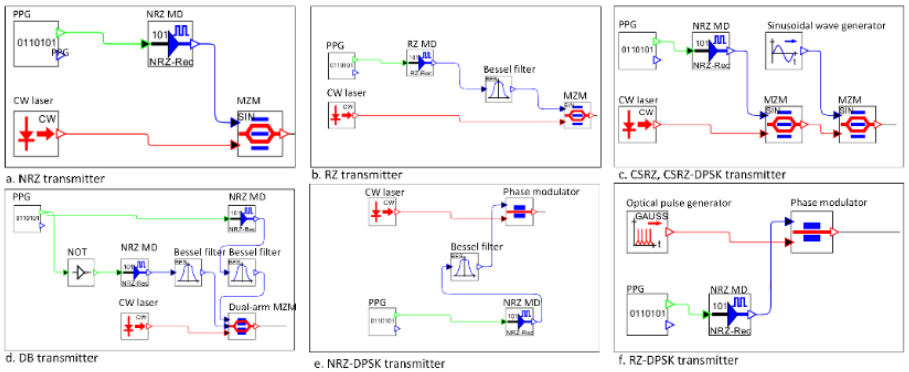

Fig. 2. Different type optical transmitters for implementation of the following modulation formats: (a) NRZ, (b) RZ, (c) CSRZ and CSRZ-DPSK, (d) DB, (e) NRZ-DPSK, and (f) RZ-DPSK.

As mentioned above, transmitters for all our investigated modulation formats are shown in Fig. 2. NRZ transmitter is shown in Fig. 2(a). It is built according to a typical NRZ transmitter structure based on MZM. Electrical signal for MZM is provided by NRZ modulator driver (MD), which forms NRZ line code according to pseudo random bit sequence from pulse pattern generator (PPG) at 10 Gbit/s bit rate. Analogically formed RZ transmitter is shown in Fig. 2(b). It is implemented by electronically generating RZ pulses and, consequently, differs from the previous transmitter only by the way, how an optical modulator is driven. There is also the Bessel filter used for signal from modulator driver filtering. The structure of CSRZ-OOK and CSRZ-DPSK transmitter is shown in Fig. 2(c). The transmitters of these formats have a similar structure although element parameters are different. The modulation of optical signal is carried out in two stages. In the first stage, MZM is used for phase or intensity modulation. Then the second stage applies an alternate-phase pulse carving to the signal. It is composed by MZM modulator driven by a sinusoidal signal with frequency equal to half of the bit rate [18]. The duobinary transmitter can be seen in Fig. 2(d). The dual-arm MZM is driven with two inverse NRZ signals prefiltered using a low-pass Bessel filter. For NRZ-DPSK and RZ-DPSK modulation the transmitters are based on phase modulator (PM) from OptSim models library. They are shown in Fig. 2(e) and Fig. 2(f) and have a similar structure. The difference is that they are accordingly driven by NRZ and RZ modulator drivers and for RZ-DPSK transmitter Super-Gaussian optical pulse generator (based on CW laser with the same parameters) is used as an optical signal source.

3. RESULTS AND DISCUSSION

As the main criterion for performance comparison of investigated modulation formats we have chosen the maximal transmission distance, which can be achieved under the defined signal quality. As threshold for maximal distance evaluation the BER less than 10^{-9} in each channel has been chosen. At first we evaluated performance of all modulation formats (NRZ-OOK, RZ-OOK, CSRZ-OOK, NRZ-DPSK, RZ-DPSK, CSRZ-DPSK and DB) in system without dispersion compensation. Maximal transmission distances obtained by each format are shown in Table 1. As one can see, the best performance is demonstrated by DB and CSRZ-DPSK – their maximal distance is more than 90 km. Results of NRZ-OOK, both OOK and DPSK are also quite good – the maximal reach is above 80 km.

Table 1

Maximal Transmission Distance of Modulation Formats in System without DCM

No.	Format	Distance (km)
1.	DB	99
2.	CSRZ-DPSK	92
3.	NRZ-OOK	82
4.	NRZ-DPSK	80
5.	CSRZ-OOK	72
6.	RZ-OOK	60
7.	RZ-DPSK	54

Table 2 demonstrates the performance of each modulation format in the system where DCF is used. As it is shown in Table 2, in the system with DCF the performance of DPSK formats is much better than performance of OOK formats. To analyse the influence of dispersion on each format performance, data about an increase of maximal reach of each format using the dispersion compensation are also summarised in Table 2. Distance increase is evaluated in relation to maximal reach without DCF. As one can see, chromatic dispersion is the main distance-limiting factor for RZ-DPSK format. For DB, on the contrary, dispersion compensation has not improved reach significantly.

Table 2

Maximal Transmission Distance of Modulation Formats in System with DCF

No.	Format	Distance (km)	DCF length (km)	Distance increase using DCF (%)
1.	RZ-DPSK	203	38	276 %
2.	NRZ-DPSK	187	37	134 %
3.	CSRZ-DPSK	166	31	103 %
4.	RZ	122	22	80 %
5.	NRZ	115	20	51 %
6.	CSRZ	109	19	40 %
7.	DB	103	7	4 %

The input spectra of all investigated modulation formats as well as input and output eye diagrams for both scenarios of transmission system are shown in Fig. 3.

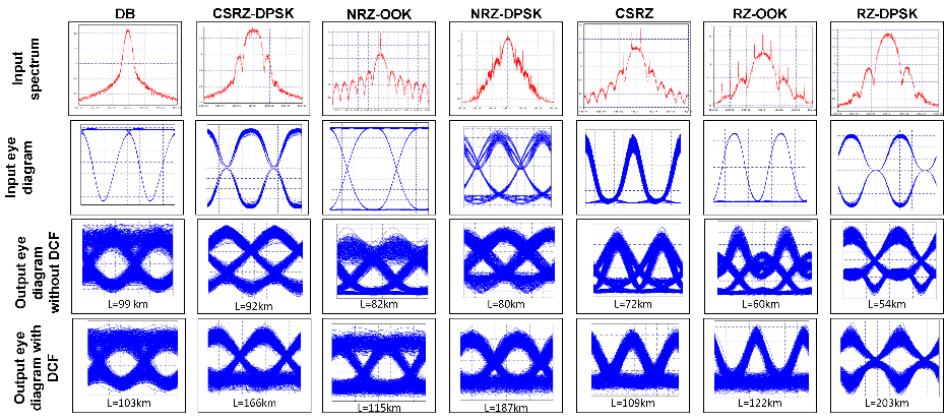

Fig. 3. Input spectra, eye diagrams and output eye diagrams at maximum achievable transmission distance in the systems without and with DCF dispersion compensation module.

In addition, the performance of three best performed modulation formats in both scenarios was evaluated by changing channel spacings. According to ITU-T G.694.1 recommendation, 25 GHz and 50 GHz spacings were investigated. The results are shown in Table 3.

Table 3

Maximal Transmission Distance of Modulation Formats in Systems without and with DCF Using 100 GHz, 50 GHz and 25 GHz Channel Spacings

No.	Format	Distance (km) Channel spacing: 100 GHz	Distance (km) Channel spacing: 50 GHz	Distance (km) Channel spacing: 25 GHz
System without DCF				
1.	DB	99	101	105
2.	CSRZ-DPSK	92	91	93
3.	NRZ-OOK	82	84	77
System with DCF				
1.	RZ-DPSK	203	190	162
2.	NRZ-DPSK	187	172	151
3.	CSRZ-DPSK	166	159	154

As one can see, transmission with 50 GHz and 25 GHz channel spacings in the system without dispersion compensation and, consequently, with smaller transmission distances has been implemented as successfully as with 100 GHz channel spacing; in some case it has shown even better results. The reason of it can be that in our case nonlinear optical effects between channels have not increased BER value, but, on the contrary, improved it. Small decrease of reach was observed in NRZ-OOK system with 25 GHz channel spacing. The decrease of transmission distance

is more significant in the system with DCF. Especially it is substantial in the NRZ-DPSK case. Results demonstrated by NRZ-DPSK using 100 GHz spacing were the best ones. However, the third best result is achieved when 25 GHz spacing is used.

4. CONCLUSIONS

The recommendations and conclusions for the next generation of WDM transmission systems are as follows.

1. The maximal reach of 16-channel WDM-PON system without dispersion compensation module (DCM) was obtained by DB and CSRZ-DPSK formats; it was more than 90 km in comparison with more than 80 km achieved by NRZ-OOK. This means that in the systems where demand on maximal transmission distance is not very high, the usage of traditional NRZ-OOK remains a good cost-effective and simple solution. If it is necessary to achieve maximal reach without using dispersion compensation, the DB and CSRZ-DPSK are potentially the most suitable formats.
2. The decrease of the channel spacing to 25 GHz has not affected maximal achievable reach in the simulated transmission systems without DCF; this means that it is possible to increase capacity as well as spectral efficiency in such kind of systems keeping maximal transmission length.
3. RZ-DPSK demonstrated the maximal achievable reach of the system (203 km) using DCF and 100 GHz channel spacing.
4. Significant increase of maximal achievable reach in 16-channel WDM-PON system with DCF has shown that chromatic dispersion is an important limiting factor of system performance.
5. However, influence of chromatic dispersion on various modulation formats is very different. It is definitely the main limiting factor for RZ-DPSK, but for DB, on the contrary, chromatic dispersion is not the main or single limiting factor.
6. If DCF is applied, the use of another modulation format (especially DPSK format) instead of NRZ-OOK can significantly increase the maximal reach of system.
7. In the system with DCF, a decrease of channel interval is appreciable. The smaller the channel spacing, the shorter the maximal reach. In comparison with 203 km achieved by RZ-DPSK using 100 GHz spacing, 50 GHz spacing enables transmission over slightly more than 190 km (RZ-DPSK), but using 25 GHz interval only over approximately 150 km.

ACKNOWLEDGEMENTS

The present research has been supported by the Latvian National Research Programme SOPHIS under grant agreement No. 10-4/VPP-4/11.

REFERENCES

1. Cisco. (2014). *Transformation through innovation: A strategy for service provider success.* Executive Summary. Available at http://www.cisco.com/c/en/us/solutions/collateral/service-provider/service-provider-strategy/white_paper_c11-690395.html
2. Saunders, J. D., McClure, C. R., and Mandel, L. H. (2012). Broadband applications: Categories, requirements, and future frameworks. *First Monday 17* (11).
3. ITU. (2011). *Applications over broadband Internet*. Available at https://www.itu.int/osg/spu/spunews/2003/oct-dec/applications.html
4. Kaminow, I. P., Li, T., and Willner, A. E. (2013). *Optical fiber telecommunications.* Volume VIB: Systems and Networks. Academic Press.
5. Muciaccia, T., Gargano, F., and Passaro, V. M. N. (2014). Review Passive Optical Access Networks: State of the Art and Future Evolution. *Photonics 4,* 323–346. *doi:10.3390/photonics1040323*
6. IDATE Research. (2014). *FTTx 2014 markets & trends*. Facts & Figures.
7. FTTH. (2014). Press release. *Fibre broadband flourishes as Switzerland joins the league of FTTH leaders.*
8. Jansons, G. (2015). *What is GPON? – Short Recap*. Available at http://www.edgetech.lv/what-is-gpon/
9. Binh, L. N. (2015). *Advanced digital optical communications.* Second edition. Munich: CRC Press.
10. Winzer, J., and Essiambre, R. (2006). Advanced optical modulation formats. *Proceedings of the IEEE 94* (5), 952–985.
11. Latal, J., Vitasek, J., Koudelka, P., Siska, P., Poboril, R., Hajek, L., Vanderka. A., and Vasinek, V. (2014). Simulation of modulation formats for optical access network based on WDM-PON. *16th International Conference in Transparent Optical Networks (ICTON),* 1–7, 6–10.
12. Agalliu, R., and Lucki, M. (2014). Benefits and limits of modulation formats for optical communications. *Optics and Optoelectronics 12* (2), 160–167.
13. Agalliu, R., and Lucki, M. (2015). System improvements in dense wavelength division multiplexing networks by using advanced optical modulation formats. *17th International Conference on Transparent Optical Networks (ICTON), 1–9. doi: 10.1109/ICTON.2015.7193511*
14. Ozolins, O., Bobrovs, V., and Ivanovs, G. (2012). DWDM-direct access system based on the fiber Bragg grating technology. *Proceedings of the 8th International Symposium on Communication Systems, Networks and Digital Signal Processing, CSNDSP 2012*, art. no. 6292669.
15. Udalcovs, A., Bobrovs, V., Trifonovs, I., and Celmins, T. (2013). Investigation of maximum distance reach for spectrally efficient WDM system with mixed data rates and signal formats. *Elektronika ir Elektrotechnika, 19* (1), 87–92.
16. Spolitis, S., Bobrovs, V., Ivanovs, G., and Gavars, P. (2012). Comparison of passive chromatic dispersion compensation techniques for long reach dense WDM-PON system. *Elektronika ir elektrotechnika 6* (122), 65–70.
17. Udalcovs, A., and Bobrovs, V. (2012). Investigation of spectrally efficient transmission for unequally channel spaced WDM systems with mixed data rates and signal formats. *Proceedings of the 8th International Symposium on Communication Systems, Networks and Digital Signal Processing, CSNDSP 2012*, art. no. 6292662.
18. *OptSim User Guide*. (2010). USA: RSoft Design Group.

19. *OSI Optoelectronics.* FCI-InGaAs-36C 10Gbps InGaAs Photodiode. World Class Products – Light Sensing Solutions. Available at http://www.osioptoelectronics.com/application-notes/OSI_Parts_Catalog.pdf
20. Udalcovs, A., Bobrovs, V., Parts, R., and Trifonovs, I. (2012). Evaluation of the maximum permissible transmission distance for the mixed-HDWDM systems. *Proceedings of the 9th International Symposium on Telecommunications, BIHTEL 2012*, art. no. 6412052.

DAŽĀDU MODULĀCIJAS FORMĀTU MAKSIMĀLI SASNIEDZAMA PĀRRAIDES ATTĀLUMA IZPĒTE WDM-PON SISTĒMĀS

I. Kurbatska, V. Bobrovs, S. Spolitis, P. Gavars, G. Ivanovs, R. Parts

K o p s a v i l k u m s

Ievērojot platjoslas pakalpojumu pieprasījuma apjoma pieaugumu piekļuves tīklos, šajā pētījumā, tika novērtēta modulācijas formātu spēja palielināt pārraides sistēmas maksimālo attālumu ar signāla kļūdas varbūtību ne augstāku par 10^{-9}. Realizējot 16 kanālu viļņgarumdales blīvētu pasīvā optiskā tīkla pārraides (WDM-PON) sistēmu, tika izpētīti tādi modulācijas formāti kā kodēšana bez atgriešanās pie nulles (non-return-to-zero (NRZ)), atgriešanas pie nulles (return-to zero (RZ)), RZ ar nesējfrekvences apspiešanu (carrier suppressed (CSRZ)), duo-binārā kodēšana (duobinary (DB)), NRZ ar diferenciālo fāzes modulāciju (NRZ differential phase shift keying (NRZ-DPSK), RZ-DPSK un CSRZ-DPSK. Simulācijas tika veiktas izmantojot OptSim programmu. Sistēmā bez dispersijas kompensāciju ar 100 GHz starpkanālu intervālu labākus rezultātus demonstrēja DB un CSRZ-DPSK formāti, to maksimālais pārraides attālums ir vismaz 90 km. NRZ-OOK maksimālais pārraides attālums ir virs 80 km. Starpkanālu intervāla nomaiņa no 50 GHz uz 25 GHz izmainīja maksimālo pārraides attālumu nebūtiski. Attiecībā uz pārraides sistēmu bez dispersijas kompensācijas var secināt, ka visperspektīvākie ir DB un CSRZ-DPSK formāti, bet atšķirība no tradicionāli izmantojamā NRZ-OOK nav pārāk lielā, tāpēc tas joprojām ir vienkāršs un ekonomisks risinājums, kad netiek izvirzītas augstas prasības attiecība uz nodrošināmo pārraides attālumu. Sistēmā ar dispersiju kompensējošo šķiedru (DCF) maksimālais pārraides attālums ir daudz lielāks - 203 km (RZ-DPSK formāts), kas liecina par to, ka dispersija būtiski ietekmē pārraides sistēmas veiktspēju. Tomēr ne visiem formātiem dispersijas kompensācija ir izšķiroša. Piemēram, DB formātam maksimālais pārraides attālums palielinājās tikai par 4%, salīdzinot ar 276% RZ-DPSK gadījumā. Pārraides sistēmā ar DCF dispersijas kompensācijas moduli starpkanālu intervāla samazināšana jau būtiski ietekmē maksimālo pārraides attālumu. Ja starpkanālu intervāls ir 50 GHz, tad nodrošināmais pārraides attālums ar BER<10^{-9} ir virs 190 km (RZ-DPSK formātam), bet ja intervāls tiek izraudzīts 25 GHz, tad maksimālais nodrošināmais attālums pārsniedz 150 km. Ja tiek pielietota dispersijas kompensācija (DCF šķiedra), tad šajā gadījumā DPSK formātu izmantošana tradicionāla NRZ-OOK vietā var manāmi uzlabot pārraides sistēmas darbību.

30.03.2016.

INFORMATION ON SUBSCRIPTION OF THE JOURNAL FOR YEAR 2016

Index: 2091 (to individual subscribers),
2092 (to collective subscribers)
Periodicity: bi-monthly

Price:

	individual subscribers	collective subscribers
per 2 months	EUR 1.50	EUR 15.00
per 4 months	EUR 3.00	EUR 30.00
per 6 months	EUR 4.50	EUR 45.00
per 8 months	EUR 6.00	EUR 60.00
per 10 months	EUR 7.50	EUR 75.00
per 12 months	EUR 9.00	EUR 90.00

Institute of Physical Energetics
Latvian reg. No. LV90002128912, Aizkraukles ielā 21,
Rīga, LV-1006, LATVIA
SEB banka
Account No LV 59UNLA 0001 5450 7025 7
Code: UNLALV2X

Contact person:

S. Ezerniece
tel. 67551732,67558694
http://fei-web.lv
ezerniec@edi.lv

LATVIAN JOURNAL of PHYSICS and TECHNICAL SCIENCES